

F14/71 2236 (Final)

322460  
FILE COPY

THE FRANKLIN INSTITUTE • Laboratories for Research and Development

Final Report  
No. F-2236

PERMANENT MAGNETIC MATERIALS

January 2, 1951 to December 31, 1953

Prepared for  
Chief of Naval Research, Department of the Navy  
Under Contract No. Nonr-01002

PROPERTY OF R.D.  
TECHNICAL LIBRARY

Approved by:

*Foster C. Nix*

Foster C. Nix  
Associate Director

Approved by:

*Nicol H. Smith*

Nicol H. Smith  
Director

Copy No. 2

THIS REPORT HAS BEEN DELIMITED  
AND CLEARED FOR PUBLIC RELEASE  
UNDER DOD DIRECTIVE 5200.20 AND  
NO RESTRICTIONS ARE IMPOSED UPON  
ITS USE AND DISCLOSURE.

DISTRIBUTION STATEMENT A

APPROVED FOR PUBLIC RELEASE,  
DISTRIBUTION UNLIMITED.

TABLE OF CONTENTS

	Page Number
ABSTRACT	v
1. INTRODUCTION	1
1.1 Purpose	1
1.2 Scope	1
1.3 Definition of Terms	1
2. SUMMARY OF THE PROJECT ACCOMPLISHMENTS	2
2.1 Introduction	2
2.2 Behaviour of Single-domain particles	3
2.3 Alloy Systems	6
3. PRESENT PROGRESS	7
3.1 The Nature of $\gamma$ -FeO	7
3.2 Shapes of Hysteresis Loops	20
3.3 Effect of Degree of Reduction on Magnetic Properties of Single-Domain Particles	43
3.4 Permanent Magnet Properties of Fe Powders	46
3.5 Alloy Powders	50
4. SUMMARY	55
REFERENCES	57

## LIST OF TABLES

Table Number	Caption	Page Number
Table 3-1	X-ray Diffraction Line Intensities for $\gamma$ -FeO and $\text{Fe}_3\text{O}_4$	12
Table 3-2	Calculated X-Ray Diffraction Line Intensities	13
Table 3-3	Iron-Oxygen Distances in Iron Oxides	16
Table 3-4	Magnetic Properties of Fe-85 Single-Domain Particle Compacts	26
Table 3-5	Anisotropy Constants of Fe-85 Specimens	29
Table 3-6	Magnetic Properties of Ferroxdure-"HP" Compacts	39
Table 3-7	Magnetic Properties of Partially Reduced Fe Powders	43
Table 3-8	Reoxidation of Single-Domain Fe Compacts	45
Table 3-9	Magnetic Properties of Fe-124 Compacts	47
Table 3-10	Expected Magnetic Properties of Single-Domain $\text{FeBe}_2$ Powders	51
Table 3-11	Properties of $\text{FeBe}_2$ Powders	54

## LIST OF FIGURES

Figure Number	Caption	Page Number
3-1	Magnetic Transformation of $\text{Fe}_3\text{O}_4$ and $\gamma\text{-FeO}$	8
3-2	Hysteresis Loops of $\gamma\text{-FeO}$ and $\text{Fe}_3\text{O}_4$ (around the Magnetic Transition at $-150$ to $-160^\circ\text{C}$ )	10
3-3	X-Ray Diffraction Pattern of FeO-114	18
3-4	$\alpha\text{-Fe}$ Line in X-Ray Diffraction Pattern of FeO-114	19
3-5	Hysteresis Loops of Fe-85 Compacts (upper curve only)	24
3-6	Normal Induction Curves of Fe-85 Compacts	25
3-7	Reduced Normal Induction Curves for Fe-85 Compacts	28
3-8	Coordinates for Pair of Single-Domain Particles	33
3-9	Configuration of Magnetic Vectors in Pairs of Single-Domain Particles	35
3-10	Effect of Maximum Applied Field on Intrinsic Coercive Force of "Ferroxdure"	40

THE FRANKLIN INSTITUTE - *Laboratories for Research and Development*

F-2236

LIST OF FIGURES (cont)

Figure Number	Caption	Page Number
3-11	Magnetic Properties of Ferroxdure "HP" Compacts	41
3-12	Demagnetizing Curves of Ferroxdure- "HP" Compacts	42
3-13	Properties of Compacts of Single- Domain Iron Powders	44
3-14	Magnetic Properties of Fe-124 Compacts	48

ABSTRACT

A summary is given of the work of this project over its three years of existence. Techniques for measuring particle diameters of the order of  $300\text{\AA}$  were studied, and the electron microscope and x-ray diffraction line broadening selected as the most suitable. As an outgrowth of this work, the effects of strain on x-ray line broadening were studied in greater detail. Low temperature annealing of carbonyl Fe was chosen as a convenient system to study for this purpose.

A technique for producing Fe particles under thoroughly controlled conditions was worked out. With this technique, it was shown that during low temperature reduction one Fe oxide crystallite produced one Fe particle. This result should make possible formation of Fe particles of controlled shape as well as size.

The interactions between single-domain particles in compacts were studied, and it was shown that local interactions between particles in clumps probably play a major role in determining the magnetic properties of the compacts. A method of taking these interactions into account was outlined, although this work really has only begun.

Estimates of the properties of  $\text{FeBe}_2$  single-domain particles have indicated that interesting permanent magnet properties might be produced. Grinding of bulk material of the proper phase did not produce small enough particles. A reduction method for producing smaller particles was suggested, but not explored sufficiently to permit an evaluation.

## 1. INTRODUCTION

### 1.1 Purpose

More and more, relationships that exist between the structures of ferromagnetic materials and their magnetic behavior are coming to light. It is the purpose of this program to study these relationships in the case of permanent magnet materials. In particular, the relationship between coercive force and particle size in fine powders will be given special emphasis.

### 1.2 Scope

To investigate the fundamental properties of permanent magnet materials.

### 1.3 Definition of Terms

The symbols used in this report will be listed and defined here:

- I Volume magnetization.
- $I_s$  Saturation volume Magnetization of a specimen for infinitely large fields.
- $I_o$  Saturation volume magnetization of the particles in a specimen.
- f Volume fraction of a specimen occupied by the ferromagnetic phase. In general  $f = I_s/I_o$ .
- $I_r$  Remanent volume magnetization, at zero applied field.
- B Magnetic induction in a specimen.

- $B_r$  Remanent induction,  $= 4\pi I_r$ .
- $H_o$  Applied magnetic field strength.
- $H'$  Total local field, usually taken  $= H_o + \frac{4\pi I}{3}$ .
- $I_c^H$  Intrinsic coercive force, for zero  $I$ .
- $B_c^H$  Coercive force, for zero  $B$ .
- $K$  Effective magnetic anisotropy energy constant, containing all contributions to anisotropy of magnetic energy.
- $\rho$  Density of specimen.
- $T_c$  Curie temperature.
- $k$  Boltzmann's constant.

## 2. SUMMARY OF THE PROJECT ACCOMPLISHMENTS

### 2.1 Introduction

This report comes at the end of three years of a program studying the magnetic properties of single domain powders conducted under ONR sponsorship. The project has been extended for several months, but for most phases of the work, this report will stand as the final report. For the next several months, work will be conducted on the reduction process used for the preparation of Fe powders, and a report will be issued then covering that work in detail.

This project has been based upon a study of the magnetic properties of single domain powders. Within this project, the work has been concentrated on two broad tasks. One is the study of the behavior of single domain particles, comparing predictions of domain theory to the experimental facts. The other involves a study of the properties of alloy systems capable of producing strong permanent magnets by reduction to single domain particles. The major accomplishment lies in the field of the first task.

## 2.2 Behaviour of Single-domain particles

The work of this first phase concentrated on single domain Fe powders. It involved the following steps:

- (1) Preparation of single domain Fe powders.
- (2) Measurement of the chemical composition and physical properties, such as particle size, density, etc., of the powders.
- (3) Measurement of the magnetic properties of suitable compacts.
- (4) Interpretation of these magnetic properties in terms of domain theory.

Early work on the project was concentrated on developing techniques for particle size analysis of this very fine powder (the single domain Fe particles are of the order of  $300\text{\AA}$  in diameter). It was shown that vapor phase sedimentation could not be used to measure the particle size because during the settling process the particles reclustered badly. This work is reported in detail in report I-2236-1. A detailed study was made of the use of three more or less complimentary techniques for studying particle sizes in this range. These involved the use of the electron microscope, the broadening of x-ray diffraction lines and the adsorption of nitrogen. This work is reported in detail in report P-2236-8. It was found that the electron microscope and x-ray diffraction techniques gave results in agreement with each other, but that the nitrogen adsorption technique was unreliable for the measurement of these particle sizes. The x-ray diffraction technique is a good rapid method for measuring comparative sizes where the particle size distributions are comparable from one powder to another, but in order to obtain complete particle size distributions the electron microscope must be used.

THE FRANKLIN INSTITUTE • *Laboratories for Research and Development*

HB-2331

The broadening of x-ray diffraction lines can be caused by lattice strains as well as by small crystallites. This effect was especially noticeable in fine carbonyl Fe. It was shown that particle size and strain broadening could be separated in "as prepared" carbonyl Fe. Annealing caused strain relief first, followed by crystal growth at higher temperatures ( $> 350^{\circ}\text{C}$ ).

For the preparation of the single domain powders, the reduction of ferrous formate was chosen as the most suitable method. A simple technique for the preparation of ferrous formate was set up (P-2236-6). Attempts to reduce the ferrous formate in a stream of hydrogen led to uncertain results, especially when the masses used involved more than a few grams of Fe (P-2236-9). Instead, a reduction technique was developed in which the ferrous formate was first thermally decomposed to an Fe oxide whose composition was approximately FeO. The FeO was then reduced at low hydrogen pressures, using calcium hydride intimately mixed with the FeO powder to absorb the  $\text{H}_2\text{O}$  produced by the reduction (P-2236-10). A detailed study of the reduction process was made in order to learn more about the factors controlling the size and shape of the final Fe powder. This study has not been completed, but will be fully reported in a special report at the conclusion of the program. The major conclusion from the work, however, is that each FeO crystallite produces one Fe particle.

The FeO resulting from the thermal decomposition of the ferrous formate has been reported to possess a spinel lattice<sup>(1)</sup>, and to contain only ferrous Fe. Evidence gained in this program, given in detail below, indicates rather strongly that this interpretation is erroneous. The magnetic properties of the oxide corresponds closely to a mixture of  $\text{Fe}_3\text{O}_4$  plus a non-magnetic phase. This phase, upon the evidence of chemical analysis, is thought to be Fe so finely divided that it does not contribute to the magnetic properties.

THE FRANKLIN INSTITUTE • *Laboratories for Research and Development*

F-2236

The degree of reduction has some influence on the magnetic properties of these single domain powders. High metal content results in a high saturation moment. On the other hand, there is not much effect noticed on the coercive force. This has been previously discussed in Quarterly Progress Report P-2236-10, and further work will be reported below. Once the single domain powders are formed, however, reoxidation does seem to be important. This is true for both the loose powders, and for the pressed specimens. The effect is most noticeable in the coercive force, but reoxidation also tends to reduce the saturation moment. Studies have been made involving the use of carefully dried benzene to preserve the powder, and impregnation of the compacts with a resin. These effects are reported in more detail here.

No real attempt has been made in this program to obtain the highest  $(BH)_{\max}$  possible. The best values obtained were for a specimen pressed at 80 tsi, and were of the order of  $0.95 \times 10^6$  ergs/cm<sup>2</sup>.

A study was made of the shapes of the hysteresis loops of compacts of these single domain Fe powders. Although this study is not complete, the results to date will be reported here. Earlier work was done on compacts of a carbonyl Fe, designated P-818, obtained through the generosity of the General Aniline and Film Corporation. The particles of this powder were approximately one micron in diameter, which is far larger than for single domain powder. Furthermore, according to the results of this study, and also according to the manufacturer, these particles tended to be agglomerated in chains several microns long. This work was reported in Quarterly Progress Report P-2236-6 and P-2236-9, and I-2236-2. The magnetization curves of these powders could be accounted for in terms of the quasi-ellipsoidal shape of the agglomerates, assuming that interaction between these clumps was through a Lorentz field. Similar studies have been made using (1) a single domain Fe, diluted with a very fine SiO<sub>2</sub> powder and pressed into compacts; and

(2) similar compacts made by mixing in various proportions a five micron carbonyl Fe with finely ground Ferroxdure. The carbonyl Fe was General Aniline and Film's "HP". Ferroxdure is a commercial oxide permanent magnet material, whose chemical composition is roughly  $\text{BaFe}_{12}\text{O}_{19}$ . This material was obtained through the generosity of the Ferroxcube Corporation. The experimental data obtained in these studies included the normal induction curve, the hysteresis loop, and the approach to saturation, as well as compact density, chemical composition etc. The interpretation of the shapes of these loops is still incomplete. A detailed report of the progress will be included here.

### 2.3 Alloy Systems

The emphasis during this program on the first phase allowed only a start on the second, involving the study of single domain alloy powders. Preliminary experiments indicated that fine powders whose compositions were close to FePt could be prepared by reduction of  $\text{FePtCl}_6$ . Coercive force of such powders was of the order of 500 Oe. This material was not explored further. Domain theory combined with what data is available in the literature indicated that powders of composition of  $\text{FeBe}_2$  should possess coercive forces of the order of several thousand Oe in the single domain range. Melts were prepared with this composition, and reduced by grinding to particles with diameters down to about a micron. For these particles, the coercive force rose to about 68 Oe for the smallest diameters. The calculations show, however, that the critical diameter for single domain behavior should be in the neighborhood of 300 Å. In order to achieve the high coercive forces possible, particles with diameters in this range would be necessary. Although the material is quite brittle it was found to be impossible to produce powders smaller than about one micron by grinding. It was planned to attempt to prepare finer particles by reducing  $\text{FeBe}_2(\text{CN})_6$ , but active work was not started. This work will be summarized in more detail below.

## 3. PRESENT PROGRESS

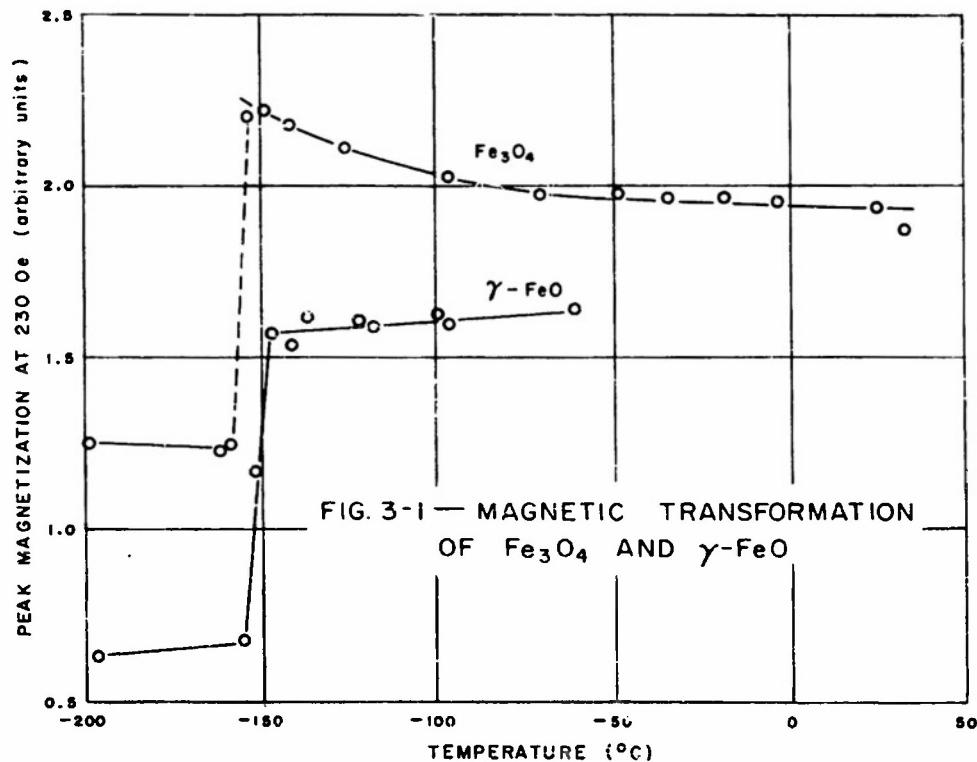
3.1 The Nature of  $\gamma$ -FeO

In the preparation of the single domain Fe powders, ferrous formate is thermally decomposed in vacuo at temperatures between 220 and 250°C. The resulting product is a black ferromagnetic powder whose particle diameter is of the order of 100 to 300 Å. The chemical composition corresponds roughly to FeO, although a considerable amount of carbon is present. This oxide has been described by Lihl<sup>(1)</sup>, who showed that the x-ray diffraction pattern was that of a spinel lattice, almost identical to  $\text{Fe}_3\text{O}_4$ . Lihl decided that this material was a new crystal modification of FeO, and named it  $\gamma$ -FeO. As was previously noted, however, our work has indicated that it is probably a mixture of  $\text{Fe}_3\text{O}_4$  and very finely divided Fe.

The specimens were analyzed chemically. The first step involved solution in 20%  $\text{H}_2\text{SO}_4$ , under a protective atmosphere of  $\text{N}_2$  or  $\text{CO}_2$  to prevent oxidation of the ferrous Fe. At this stage, the carbon was observed as an insoluble black powder which could be filtered off and weighed. The carbon content was about 1 wt. %. Upon ignition of the asbestos filter used, this black powder disappeared completely. The  $\text{H}_2\text{SO}_4$  solution containing the dissolved specimen was analyzed for ferrous ion by titrating with  $\text{KMnO}_4$ , and for ferric ion by adding KI and back titrating with  $\text{Na}_2\text{S}_2\text{O}_3$  in the presence of starch as an indicator.

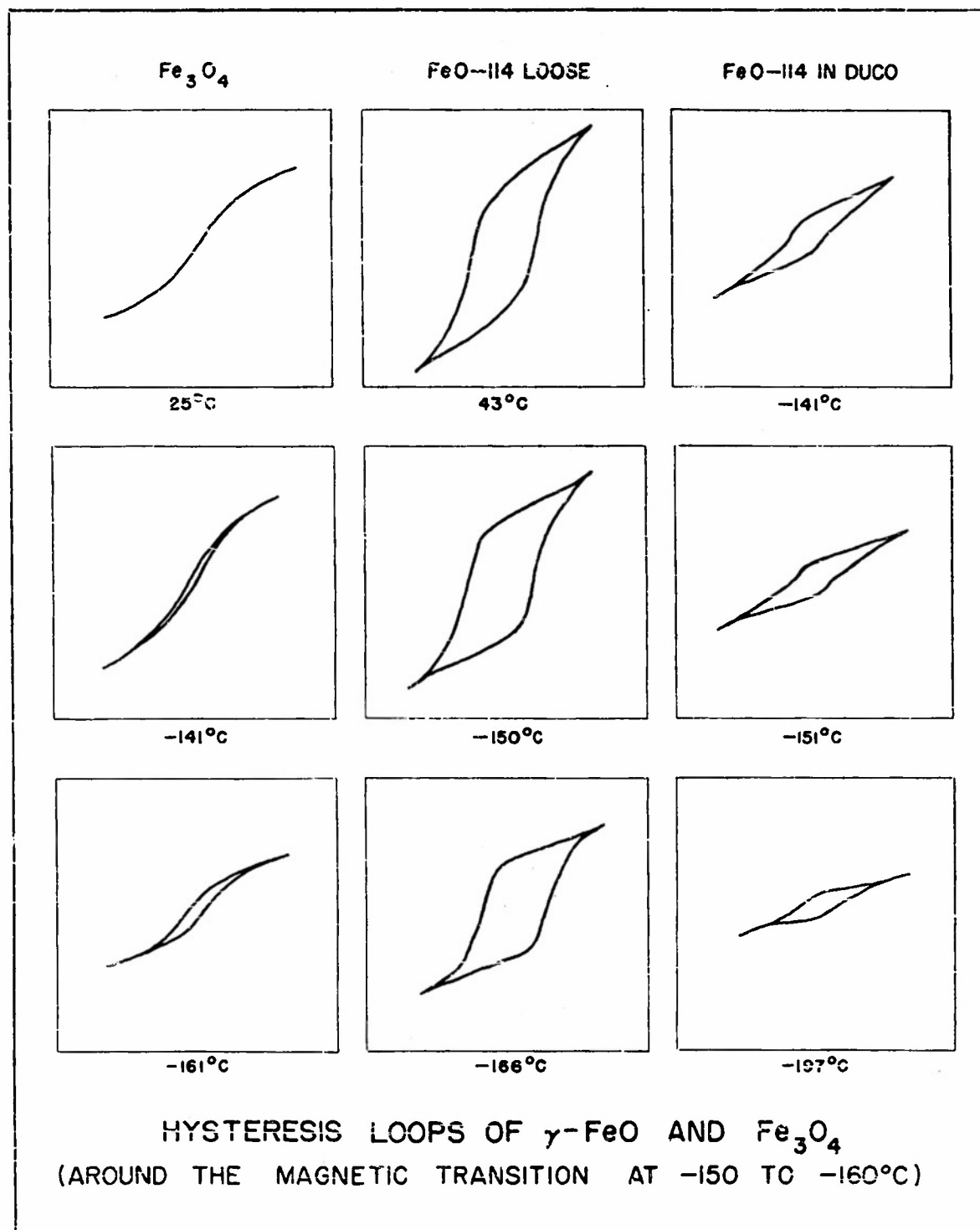
One specimen, FeO-114, was found on analysis to contain 96% FeO, and 3%  $\text{Fe}_2\text{O}_3$ . This corresponds to a composition  $\text{Fe}_{0.99}\text{O}$ . The Curie point of this specimen, sealed in vacuum in a Vycor tube, was measured in a BH curve tracer. The high coercive force (approximately 200 Oe) arising from the fine particle size, and the small sample available made the measurements rather imprecise. The Curie temperature was observed

to lie between 530° and 580°C. The Curie point of  $\text{Fe}_3\text{O}_4$ <sup>(2)</sup> is about 578°C, so that FeO-114 possesses a Curie point in the same range as does  $\text{Fe}_3\text{O}_4$ . At low temperatures (about -160°C),  $\text{Fe}_3\text{O}_4$  exhibits a magnetic transition in which the magnetization measured at intermediate fields suddenly drops in magnitude. Verwey and Haayman<sup>(3)</sup> attributed this transition to the development of order among the electrons on the ferrous and ferric ions occupying the octahedral lattice sites in the spinel structure. This transition is quite typical of  $\text{Fe}_3\text{O}_4$  and ferrites possessing ions with several oxidation states. When one considers the electronic interpretation of the mechanism of this transition, one should not expect it to appear in the  $\gamma$ -FeO, since this possesses only ferrous ions. However a very distinct transition was found in FeO-114. Figure 3.1



shows the data for the peak magnetization measured in the curve tracer as a function of temperature for both a powdered  $\text{Fe}_3\text{O}_4$  and for  $\text{FeO-114}$ . The peak field strength in the curve tracer was about 230 Oe. Because of the high coercive force of  $\text{FeO-114}$ , the magnetization values observed were very much lower than those found with the  $\text{Fe}_3\text{O}_4$ , but the transition shows quite distinctly in both, at about the same temperature, and with a drop in magnetization of about the same relative amount. Because of the high coercive force of the  $\text{FeO-114}$ , loose powders simply packed in a tube tended to rotate physically to follow the field. This tendency obscured the transition somewhat. However, by fixing the particles in Duro cement, it was possible to prevent this rotation, and the data in Figure 3-1 was obtained. A distinct change in the shape of the hysteresis loop took place as the material passed through this transition. Figure 3-2 shows the hysteresis loops observed for the  $\text{Fe}_3\text{O}_4$ , loose  $\text{FeO-114}$ , and fixed  $\text{FeO-114}$ , at temperatures above and below the transition. In each case, there is a marked change, in which the loop becomes more square, and a general lowering of the average slope of the loop occurs. This is visible even with loose  $\text{FeO-114}$ . For  $\text{FeO-114}$ ,  $-151^\circ\text{C}$  is the middle of the transition.

A second specimen of this  $\gamma\text{-FeO}$  was compressed into a bar at 12 tsi. Chemical analysis indicated that the Fe was present as a mixed oxide corresponding to 86 wt %  $\text{FeO}$  and 14 wt %  $\text{Fe}_2\text{O}_3$ . The saturation moment of a pressed bar of this material was measured in the permeameter, and was converted to magnetic moment per Fe atom using the density and chemical composition of the bar. Since the Curie point of this material is about the same as that for  $\text{Fe}_3\text{O}_4$ , this magnetic moment was extrapolated to  $0^\circ\text{K}$  by assuming the same ratio of the moment at room temperature to that at  $0^\circ\text{K}$  as is found in  $\text{Fe}_3\text{O}_4$ . Bozorth<sup>(2)</sup> gives 0.94 for this ratio. The resulting moment per Fe atom is 0.97 Bohr magnetons. The composition of this material corresponds to  $\text{Fe}_{3.76}\text{O}_4$ . If only three of these Fe ions contribute to the magnetic moment, then the moment for the  $\text{Fe}_3\text{O}_4$



would be 1.2 magnetons per Fe ion, compared to 1.33 normally found in  $\text{Fe}_3\text{O}_4$ . These values are equal within the error introduced by the approximations of this rough calculation.

The magnetic properties observed, including Curie point, magnetic transition and saturation moment indicate that the ferromagnetic phase present is  $\text{Fe}_3\text{O}_4$ . The chemical analysis indicates that extra Fe must be present. The lack of contribution from this extra Fe to the magnetic properties may be due to its very fine particle size. The number of effective near neighbors might be too low to maintain ferromagnetism.

X-ray diffraction studies of this  $\gamma\text{-FeO}$  indicate that its pattern is almost identical to that of  $\text{Fe}_3\text{O}_4$ . Table 3.1 presents the intensities of the observed lines for two different  $\gamma\text{-FeO}$  samples and for  $\text{Fe}_3\text{O}_4$ , for the latter both observed and calculated from the known structure. This data was obtained using a G. E. XRD-3 spectrometer with a Fe tube and an Mn filter. The powders were either pressed in briquettes or pressed loosely into a brass holder. The intensities listed in the table are peak intensities. The lines for the FeO samples were quite broad, consistent with the fine particle size, so that the intensities are not as certain as for the  $\text{Fe}_3\text{O}_4$  specimen. Within the error introduced by this uncertainty the patterns for the  $\gamma\text{-FeO}$  are identical to that of the  $\text{Fe}_3\text{O}_4$ , except that the lattice constant of the  $\gamma\text{-FeO}$  appears to be about 0.1% smaller than that of  $\text{Fe}_3\text{O}_4$ . Lihl<sup>(1)</sup> also reported a lattice constant for  $\gamma\text{-FeO}$  smaller by about 0.1% than that of  $\text{Fe}_3\text{O}_4$ .

A more detailed comparison was made of the observed intensities from FeO-114 with those expected for various possible structures corresponding to the chemical composition FeO, maintaining the appropriate symmetry. This composition could be realized in one way by adding extra Fe ions to the  $\text{Fe}_3\text{O}_4$  structure. The unit cell for the  $\text{Fe}_3\text{O}_4$  consists of 32 oxygen ions arranged in a face-centered cubic lattice, with the 24 Fe ions distributed in a regular fashion among the interstices between the

TABLE 3.1

X-ray Diffraction Line Intensities for  $\gamma$ -FeO and  $\text{Fe}_3\text{O}_4$ 

Line (hkl)	FeO-1	FeO-114	$\text{Fe}_3\text{O}_4$ obs.	$\text{Fe}_3\text{O}_4$ calc.
111	5	---	7	6.4
220	24	26	25	28.6
311	100	100	100	100.0
222	3	5	6	7.0
400	23	22	17	20.6
422	6	12	4	9.3
333	18	23	16	29.6
511				
440	26	30	25	46.0
533	4	---	3	12.4
553	7	---	9	14.0

oxygen atoms. There are many unoccupied interstices in the  $\text{Fe}_3\text{O}_4$  structure, into which the extra Fe ions might fit. An alternative way of maintaining the appropriate symmetry and arriving at the observed composition of the  $\gamma$ -FeO would be to allow 24 Fe ions per unit cell, as in  $\text{Fe}_3\text{O}_4$ , and to have vacancies in the oxygen lattice. The first structure would correspond to a unit cell expressed as  $\text{Fe}_{32}\text{O}_{32}$ , and the second to a unit cell expressed as  $\text{Fe}_{24}\text{O}_{24}$ . In Table 3.2 the observed intensities of FeO-114 are listed and compared to the intensities calculated for various arrangements of the Fe and oxygen ions in these two schemes.

F-2236

TABLE 3.2  
Calculated X-Ray Diffraction Line Intensities

Line (hkl)	$\text{Fe}_3\text{O}_4$ (calc.)	FeO-114	$\text{Fe}_2\text{O}_3$	A	B	C	D	E
111	6.4	---	6.4	6.2	---	1.4	6.2	12.7
220	28.6	26	28.6	57.2	84.0	36.2	28.6	23.7
311	100.0	100	100.0	100.0	100.0	100.0	100.0	100.0
222	7.0	5	12.5	68.0	36.6	26.4	14.3	7.9
400	20.6	22	15.7	48.9	22.8	15.1	8.2	6.3
422	9.3	12	9.3	18.6	27.5	11.8	9.3	7.7
333	29.6	23	29.6	29.6	29.6	29.6	29.6	29.6
511								
440	46.0	30	40.9	140.6	114.0	102.8	88.6	79.4
533	12.4		12.4	12.4	12.4	12.4	12.4	12.4
553	14.0		14.0	14.0	14.0	14.0	14.0	14.0

The first column lists the diffraction line. The second column gives intensities calculated for  $\text{Fe}_3\text{O}_4$ . The third column gives the observed intensities for FeO-114. The fourth column gives the intensities calculated for the  $\text{Fe}_{24}\text{O}_{24}$  unit cell, in which oxygen vacancies are randomly arranged. In columns five to nine headed A to E, are listed intensities calculated for various arrangements of the Fe ions in a  $\text{Fe}_{32}\text{O}_{32}$  unit cell, consistent with cubic symmetry.

In the usual spinel lattice, there are 32 octahedral and 64 tetrahedral interstices. Of these, 16 octahedral and 8 tetrahedral are occupied in  $\text{Fe}_3\text{O}_4$ . For the  $\text{Fe}_{32}\text{O}_{32}$  unit cell, 8 ferrous ions must be added. In the fourth column, under the heading A, all these extra ferrous ions are in the octahedral sites. Under B, they are divided in a ratio of 2:1 octahedral to tetrahedral. Under C, the ratio is 4:4; under D it is 16:56, which corresponds to a random distribution; under E, all 8 extra ferrous ions are in the tetrahedral sites. The ions assigned to the two types of sites are distributed at random within each type in these models. For these  $\text{Fe}_{32}\text{O}_{32}$  lattices, the (440) line is very sensitive to the presence of the extra Fe ions, and appears to rule out any of these models, since this is a strong line and the intensity disagreements are far beyond experimental error. Similar calculations were made for the 4:4 ratio in which the extra ferrous ions were put into the two classes of interstices in various ordered fashions consistent with the cubic symmetry. In every case, the (440) line disagreed with the observed intensity quite strongly. These results make it seem probable that a  $\gamma$ -FeO structure with a unit cell  $\text{Fe}_{32}\text{O}_{32}$  is not present.

For the unit cell containing oxygen vacancies, corresponding to  $\text{Fe}_{24}\text{O}_{24}$ , there is little change in the intensities from  $\text{Fe}_3\text{O}_4$ . The one exception seems to be the (222) line, in which the calculated intensity is approximately twice the observed. This discrepancy appears to

make this structure very improbable. Lihl's<sup>(1)</sup> interpretation of the properties of this material called for the presence of the carbon observed in the chemical composition to stabilize the lattice. This carbon perhaps could occupy the oxygen vacancies. However, his chemical analysis would correspond to a unit cell  $\text{Fe}_{24}\text{O}_{21}\text{C}_{3.2}$ , and would still require 7.5 oxygen vacancies per unit cell. The presence of this many vacancies in such a lattice seems highly unlikely.

The cell constant observed for the  $\gamma$ -FeO is slightly smaller than that for  $\text{Fe}_3\text{O}_4$ . This again would tend to eliminate any  $\text{Fe}_{32}\text{O}_{32}$  structure, in which the oxygen lattice as found in  $\text{Fe}_3\text{O}_4$  remains intact while additional Fe ions are put into the interstices. This is so because the ferrous ion is larger than the ferric ion, and is indeed too large to fit comfortably into the tetrahedral interstices. Insertion of the extra ferrous ions into tetrahedral sites should expand the lattice, not contract it.

Table 3.3 gives the observed and calculated Fe-oxygen distances in  $\text{Fe}_3\text{O}_4$  and  $\alpha$ -FeO. The calculations were made using ionic radii taken from Wyckoff<sup>(4)</sup>. These radii are

$\text{Fe}^{2+}$	0.80 Å
$\text{Fe}^{3+}$	0.67 Å
$\text{O}^{2-}$	1.35 Å.

The cell constants were taken as 8.39 Å for  $\text{Fe}_3\text{O}_4$  and 4.33 Å for  $\alpha$ -FeO.

TABLE 3.3

## Iron-Oxygen Distances in Iron Oxides

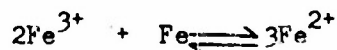
Compound	Position	Obs.	Calc.
$\text{Fe}_3\text{O}_4$	Tetra- $\text{Fe}^{3+}$	1.82 Å	2.02 Å
$\text{Fe}_3\text{O}_4$	Tetra- $\text{Fe}^{2+}$	--	2.15
$\text{Fe}_3\text{O}_4$	Octa- $\text{Fe}^{3+}$	2.10	2.02
$\text{Fe}_3\text{O}_4$	Octa- $\text{Fe}^{2+}$	2.10	2.15
$\alpha\text{-FeO}$	Octa- $\text{Fe}^{2+}$	2.16	2.15

The first column lists the oxide, the second column gives the position occupied by the Fe ion, the third column gives the observed Fe-oxygen distances, and the fourth column gives the distances calculated on the basis of the ionic radii, using the appropriate ions listed in the second column. In  $\text{Fe}_3\text{O}_4$ , both the  $\text{Fe}^{2+}$  and  $\text{Fe}^{3+}$  ions fit reasonably well into the octahedral sites, but both are definitely larger than the available space in the tetrahedral sites. Since the  $\text{Fe}^{2+}$  ions have larger radii than do the  $\text{Fe}^{3+}$  ions, conversion of the  $\text{Fe}^{3+}$  ions in the tetrahedral sites to  $\text{Fe}^{2+}$ , as required for  $\gamma\text{-FeO}$ , would result in even greater misfit and should produce a cell constant greater than that of  $\text{Fe}_3\text{O}_4$ . This effect is illustrated in the comparison between  $\text{Fe}_3\text{O}_4$  and  $\alpha\text{-FeO}$ . The  $\alpha\text{-FeO}$  possesses the same oxygen lattice as  $\text{Fe}_3\text{O}_4$ , but all of the  $\text{Fe}^{2+}$  ions are in octahedral sites. The oxygen lattice expands slightly, and there is very little misfit between the observed and calculated distances. Since the magnetic moment for each unit cell of 32 oxygen atoms is about the same in the  $\gamma\text{-FeO}$  as in  $\text{Fe}_3\text{O}_4$ , the current explanation of the magnetic properties of spinels given by Néel<sup>(5)</sup> would

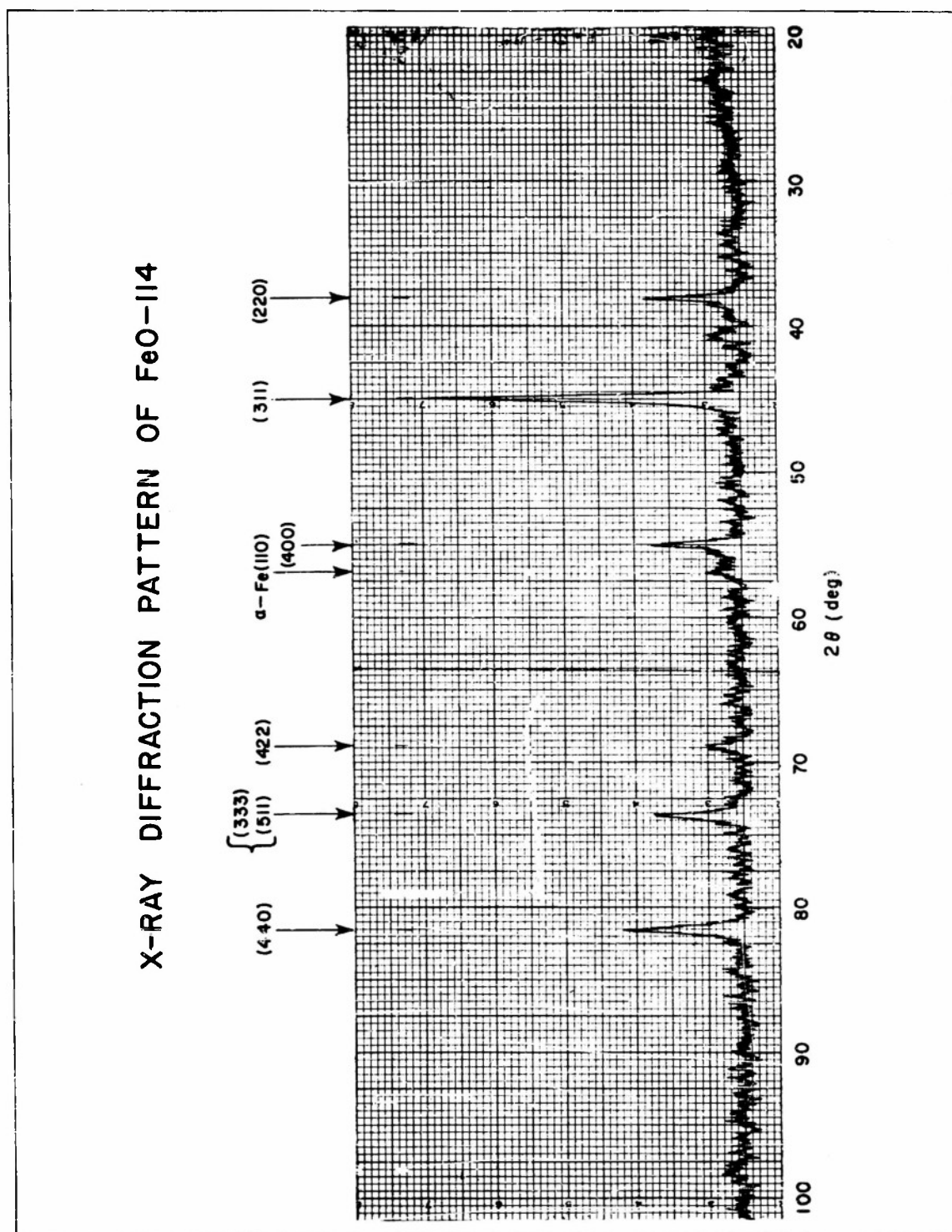
require that four of the extra  $\text{Fe}^{2+}$  ions be distributed in the tetrahedral sites and four in the octahedral sites. It thus appears that an  $\text{Fe}_{32}^{0.32}$  unit cell should be larger than  $\text{Fe}_3\text{O}_4$ , in contradiction to the observation that the cell constant of the  $\gamma$ -FeO is slightly smaller than that of  $\text{Fe}_3\text{O}_4$ .

All of the evidence presented thus far suggests that the  $\gamma$ -FeO in reality is a mixture of  $\text{Fe}_3\text{O}_4$  and Fe, with the Fe present in extremely small particles and non-ferromagnetic. A re-examination of the x-ray diffraction patterns of FeO-114 was made, and the presence of the strong (110)  $\alpha$ -Fe line was observed, although the line was very broad and very low. Fig. 3-3 shows the entire x-ray diagram for FeO-114 with the  $\alpha$ -Fe line indicated. In Fig. 3-4 the pattern in the immediate vicinity of this line was drawn on the spectrometer with the Geiger counter driven at slow speed. The  $\alpha$ -Fe line shows quite distinctly as a low, broad, diffraction line. It should be noted that this line is close to the background, and did not appear distinctly in every pattern. However, it appeared enough (in about 75%) to be unmistakable. The appearance of this line is quite consistent with an extremely small particle size.

It remains to explain why the chemical analysis did not show the presence of this metallic Fe, either in the work here or in Lihl's work. During the initial step of the chemical analysis, the powders were dissolved in an acid solution. The presence of ferric ion in the solution immediately surrounding the particle should have an oxidizing effect upon the metallic ion according to the equation.

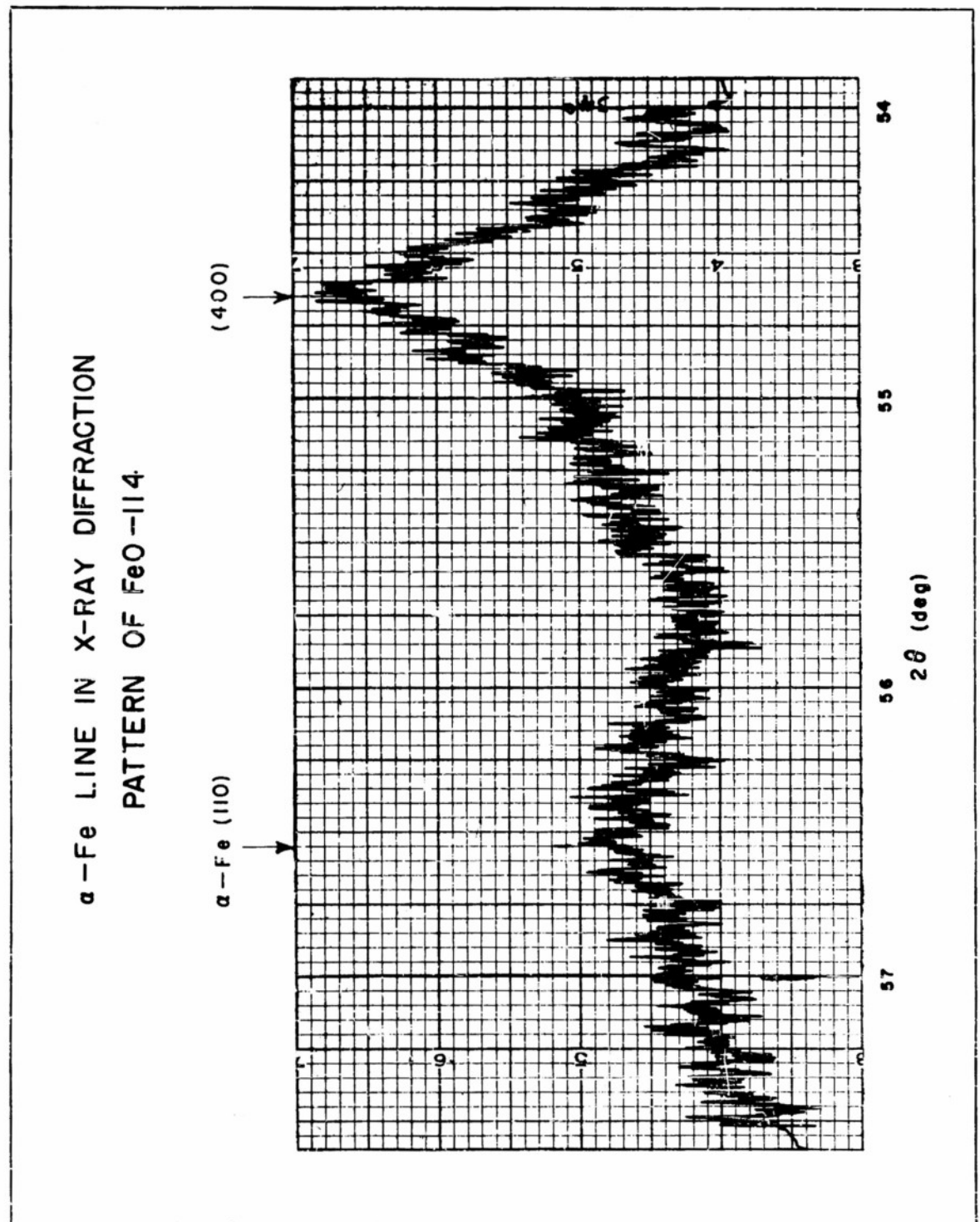


Since dissolution of the powder in acid is also the step used to determine the presence of metallic Fe by measuring the amount of hydrogen evolved, this proposed reaction would not only mask the presence of ferric ion but also the presence of metallic Fe. In an attempt to check this effect,



REPORT F-2236

FIGURE 3-3



REPORT F-2236

FIGURE 3-4

the hydrogen evolution technique was repeated with a powerful complexing agent for ferric ion, Versene, added to the acid solution. Under these conditions, the ferric ion should be stabilized, and its tendency to oxidize the metallic Fe reduced. Without the Versene, hydrogen evolution indicated the presence of < 0.5 Wt. % metallic Fe in FeO-114. No  $H_2$  was evolved. The quoted figure is the sensitivity of the method. With the Versene, the concentration of metallic Fe appeared to be about 2%. This difference is beyond experimental error, and indicates that indeed metallic Fe was present in FeO-114. The fact that the percentage observed was so low is probably due to incomplete complexing of the ferric ion by the Versene. Thermodynamic calculations show that even with the versene, the combination of  $Fe^{3+}$  + metallic Fe should be unstable with respect to  $Fe^{2+}$ .

Taken altogether, the evidence seems to indicate quite strongly that the so-called  $\gamma$ -FeO is in reality a mixture of  $Fe_3O_4$  and metallic Fe.

### 3.2 Shapes of Hysteresis Loops

#### 3.2.1 Introduction

Until fairly recently, magnetic interactions between domains have been neglected in theoretical models of ferromagnetic materials. In single crystals this is justifiable, since continuity of crystalline axes throughout the specimen allows the magnetization within the domains to be arranged so that the divergence of the magnetization is everywhere zero, and no internal demagnetizing field exist. In polycrystalline materials, on the other hand, this is not necessarily possible, and the effects of internal demagnetizing fields must be considered. The local fields acting upon the domain become very uncertain, and precise calculation difficult.

Neel<sup>(6)</sup> and Lawton and Stewart<sup>(7)</sup> have suggested that the magnetization of all grains is actually the same within a specimen, and the local fields are adjusted to make this possible. By taking the applied field as the average over the specimen, they were able to calculate the normal induction curve of a sheet of silicon-iron, with only rough agreement with experiment. Neel<sup>(8)</sup> and Holstein and Primakoff<sup>(9)</sup> have taken the inter-grain interactions into account in the approach to saturation. The treatment of the shapes of normal induction curves and hysteresis loops of polycrystalline specimens is only very rudimentary, and needs much more work.

The magnetization process in single-domain particles is particularly simple, since only rotation of the magnetic vector can occur. By studying the changes in magnetic properties as the conditions of assembling collections of these particles are varied, it should be possible to learn more of the magnetic interaction between the particles. Stoner and Wohlfarth<sup>(10)</sup> have calculated in detail the necessary equations for the behavior of non-interacting single-domain particles. The basic problem in accounting for the magnetic properties of compacts of such particles is to bring in the effect of their interaction. In principle this should be possible in a straightforward way provided one could specify completely the position and orientation of each particle, and provided one could handle the equations involved. Since both requirements are clearly impossible, it seems probable that some form of internal field theory must be used. In this approach, the interactions are lumped together into an internal field that is exerted upon a particular particle and that is added to the applied field. The properties of the compact are then equated to those of a collection of randomly oriented particles subject to this total field.

In earlier work on this project (P-2236-6, P-2236-9, I-2236-2), this approach was applied to compacts formed by pressing a poly-domain carbonyl Fe powder (General Aniline and Film Corp. P-818) with varying

amounts of silica powder. The shapes of the hysteresis loops of the very dilute specimens could reasonably be accounted for in terms of quasi-ellipsoidal particle clumps and a Lorentz internal field. The use of a Lorentz field must be viewed with suspicion, however. This field is obtained theoretically by dividing the contribution to the total field at the particle in question into three parts:

$$H_1 = H_0 + H_1 + H_2$$

$H_0$  is the applied field, corrected for any macroscopic demagnetization due to specimen shape.  $H_1$  is the contribution from the material beyond a certain spherical boundary, and  $H_2$  that from within this boundary. The spherical boundary is a fiction; it is drawn with the particle at the center, and large enough in extent so that the material beyond it can be treated as a continuum.  $H_1$  is simply and rigorously calculated:

$$H_1 = \frac{4\pi I}{3}$$

$H_2$  is in general not easy to calculate. For the special cases in which the moments of the volume elements within the sphere are arranged with spherical or cubic symmetry,  $H_2$  is zero. The internal field in this case is the Lorentz field

$$H = H_0 + \frac{4\pi I}{3}$$

For compacts of magnetized particles, there must exist a correlation between the direction of the moment of a given particle and the arrangement of the moments of the neighboring particles. In general then, the spherical symmetry of the moments required for the calculation of  $H_2$  as zero is not to be expected. Provided that the specimen be sufficiently dilute magnetically, this correlation may be weak enough to disregard. This is probably the reason the Lorentz field achieved a limited success in the case of the carbonyl Fe particles treated previously.

With the single-domain particles, the situation must be more complicated. Since each particle is permanently magnetized, the forces tending to hold the particles together must be very strong. It should be expected that the particles would be distributed as clumps rather than as particles. This in turn suggests that the magnetizing units could be taken as the clumps, and interaction between them accounted for with an internal field.

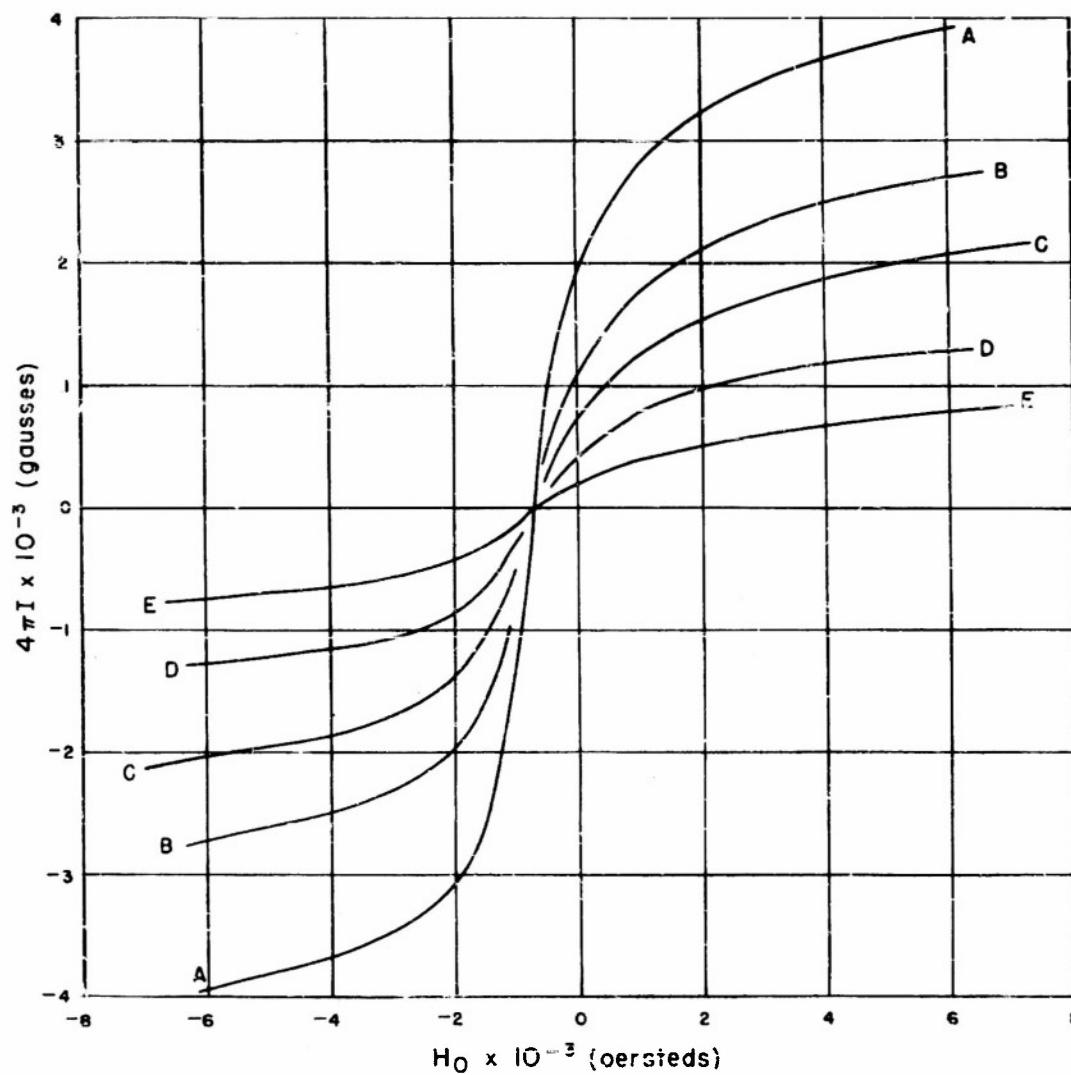
Two sets of experiments can be reported here. One series of compacts was prepared consisting of a single-domain Fe powder diluted with various amounts of a fine silica powder. Another similar series was prepared from a finely divided sample of Ferroxdure (a permanent magnet material of composition  $\text{BaFe}_{12}\text{O}_{19}$ , obtained through the generosity of the Ferroxcube Corp.) mixed with varying amounts of a polydomain carbonyl Fe powder (General Aniline and Film Corp. "HP"). The data on these two series of experiments can be presented, together with some observations on the magnetic behavior, and some preliminary results on comparing the magnetic behavior of the single-domain Fe with Lorentz-field predictions. The results of these considerations are mostly negative. An understanding of the magnetic behavior has only just begun.

### 3.2.2 Single-Domain Iron Studies

The single-domain Fe powder, Fe-85, had a particle diameter of about 200 Å. As prepared, it was about 60% pure metal, the rest being unreduced oxide. It was ball-milled briefly with various amounts of silica powder possessing a particle diameter of about 50 Å, under benzene. The mixtures were transferred to acetone, a small amount of Duco cement added, the acetone drained off and compacts pressed at 12 tsi. The magnetic measurements were made in a Sanford-Bennett<sup>(11)</sup> high-H permeameter on compacts 1/4 in x 1/4 in x 1 in.

Figures 3.5 and 3.6 give the upper half of the hysteresis loops and the normal induction curves, respectively, of the samples. In

HYSTERESIS LOOPS OF Fe-85 COMPACTS  
(UPPER CURVE ONLY)



NORMAL INDUCTION CURVES  
OF Fe-85 COMPACTS

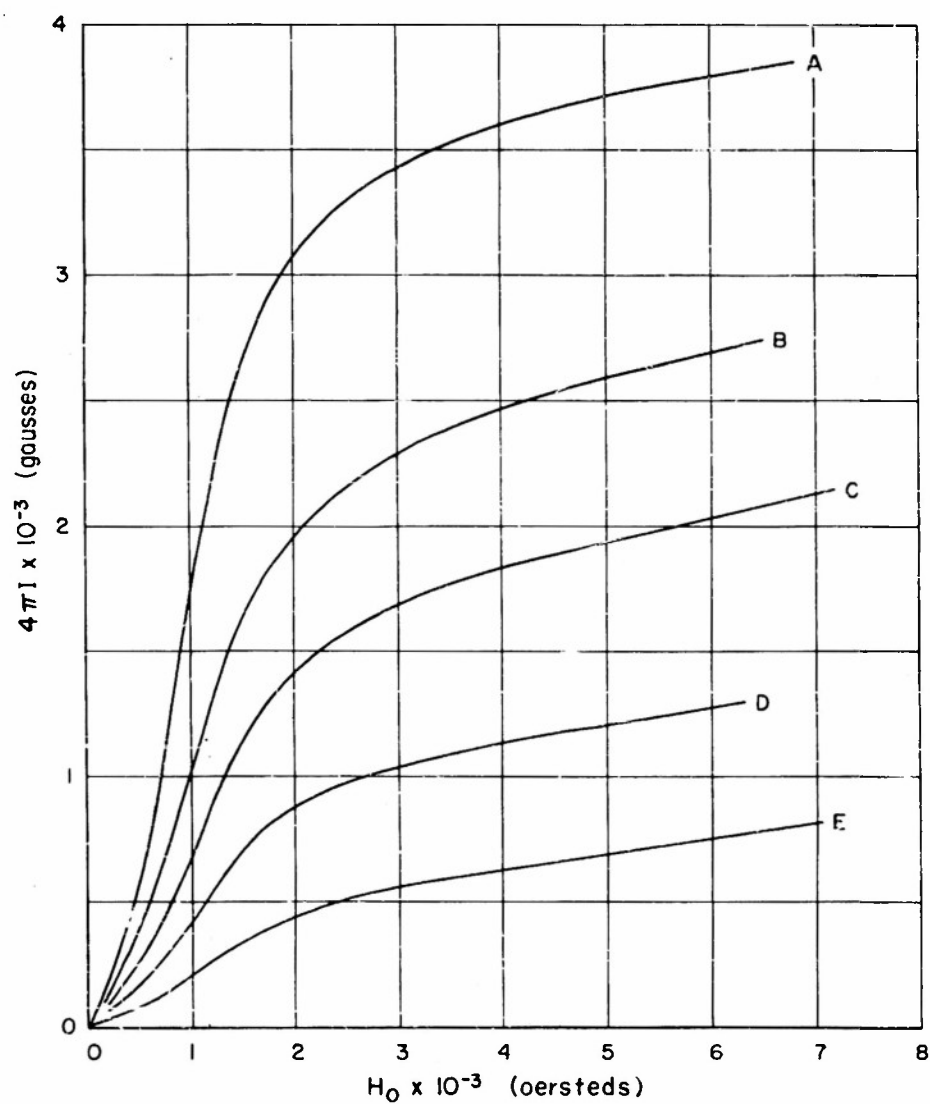


Table 3-4 are listed the properties of the specimens.

TABLE 3-4

## Magnetic Properties of Fe-85 Single-Domain Particle Compacts

Specimen	Composition	$4\pi I_s$	$4\pi I_r$	$I_H C$	$\rho$	f	$I_r/I_s$
	Wt % Fe-85	gausses	gausses	Oersteds	$g/cm^3$		
A	100	3973	1873	680	2.484	.41	.43
B	87	3044	1091	707	2.111	.31	.36
C	75	2357	735	638	2.079	.24	.31
D	50	1496	428	630	1.536	.15	.29
E	30	985	177	581	1.253	.10	.18
F	0	0	0	---	1.06	0	0

The values of saturation magnetization in the third column were obtained by extrapolation of plots of  $4\pi I$  against  $1/H^2$  to infinite field strength.

The volume fractions listed in column 7 were derived from the saturation magnetization  $4\pi I_0$  of the powder itself:

$$f = \frac{4\pi I_s}{4\pi I_0}$$

This in turn was estimated as  $4\pi I_0 = 9800$  by considering the densities and saturation moments of the samples. It is necessarily a rough value, good to no better than 10%. This is a surprisingly low value, compared to 22,400 for pure Fe, and indicates that extensive reoxidation of the specimen took place during the specimen preparation.

The magnetic behavior of these specimens was not that expected for collections of single-domain particles interacting through any simple internal field. This latter model would not produce any irreversible change in magnetization in the region of positive fields when descending from saturation. Experimentally, irreversible changes clearly occurred

in this region. Stoner and Wohlfarth<sup>(10)</sup> have shown that the ratio of remanent to saturation magnetization,  $I_r/I_s$ , should be 0.5 for randomly oriented single-domain particles. Experimentally, this ratio was close to this figure for the specimen containing only the Fe-85 powder. For the others, the ratio decreased approximately as the volume fraction occupied by the Fe-85 powder,  $f$ . Finally, Neel<sup>(12)</sup> has shown theoretically, and Weil's<sup>(13)</sup> experiments tend to agree, that the coercive force should increase linearly as the volume fraction  $f$  decreases for single-domain particles. Experimentally, the coercive force observed for these specimens remained almost constant.

As a first approximation, the behavior of these specimens was compared to that expected for a collection of single-domain particles, interacting through the Lorentz field. Stoner and Wohlfarth<sup>(10)</sup> have shown that for such a collection, the initial portion of the normal induction curve should be given by:

$$I/I_s = \frac{I_0 H'}{3K}$$

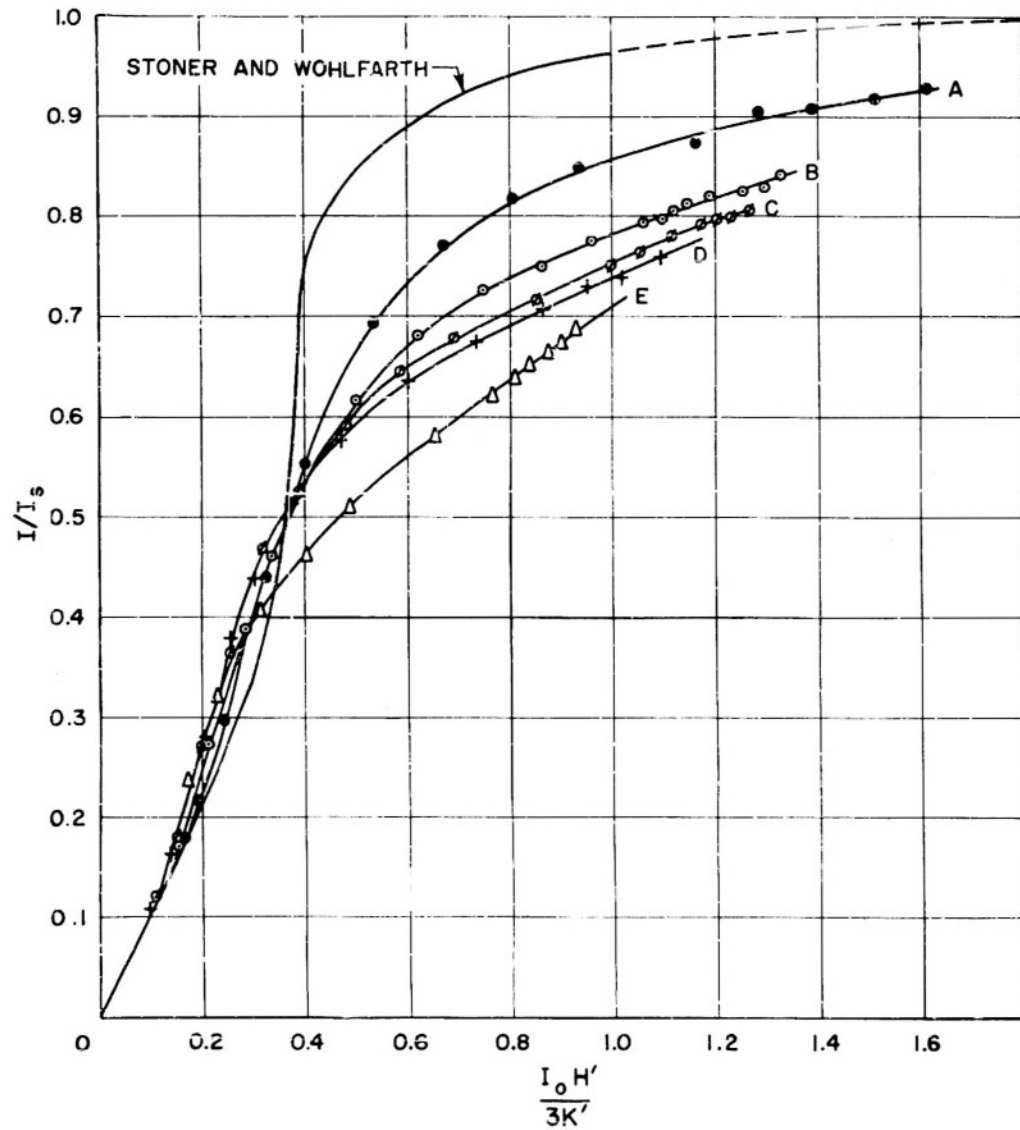
where the effective field has been chosen as:

$$H' = H_0 + \frac{4\pi I}{3}$$

The initial slopes of these plots were used to calculate effective anisotropy constants for each specimen. The fields  $H'$  were then corrected for the factor  $\frac{I_0}{3K}$ , and plots of  $I/I_s$  against this corrected field made. These are displayed in Figure 3-7. The solid line refers to theoretical values given by Stoner and Wohlfarth<sup>(10)</sup> for a randomly oriented collection of single-domain particles. The expected behavior of these specimens, if they were behaving truly as single-domain particles, would be for the data for all specimens to fall upon the Stoner and Wohlfarth curve in this reduced plot.

This discrepancy may be further pointed up by comparing the anisotropy constants derived from the initial slope, as above; from the approach to saturation; and from the coercive force. Becker and Doring<sup>(14)</sup> have shown that the approach to saturation for a non-interacting randomly oriented collection of uniaxial domains may be expressed as

# REDUCED NORMAL INDUCTION CURVES FOR Fe-85 COMPACTS



$$I = I_s \left[ 1 - \frac{8K^2}{105 I_o^2 H^2} \right]$$

Néel<sup>(8)</sup> and Holstein and Primakoff<sup>(9)</sup> have shown that this expression must be corrected for interaction when  $\alpha = \frac{4\pi I_s}{H} > 1$ . In the case here,  $\alpha$  is no larger than 0.5 at the high field strengths and for the most concentrated specimen. For the less concentrated, it falls to 0.1. In the present rough calculations, this correction was neglected.  $K$  was calculated from the slope of plots of  $4\pi I$  against  $H^{-2}$ , which were linear within experimental error for the highest field strengths, above about 5000 Oe.

An anisotropy constant can also be calculated from the intrinsic coercive force. Stoner and Wohlfarth<sup>(10)</sup> give for this coercive force for the randomly oriented uniaxial single domain particles:

$$I_c^H = \frac{0.64K}{I_o}$$

Values for these anisotropy constants are compared in Table 3-5.

TABLE 3-5

## Anisotropy Constants of Fe-85 Specimens

Specimen	Composition	$K_1$	$K_2$	$K_3$	$I_c^H$
		ergs/cm <sup>3</sup>	ergs/cm <sup>3</sup>	ergs/cm <sup>3</sup>	Oe
A	100 Wt % Fe	$1.2 \times 10^6$	$5.1 \times 10^6$	$.84 \times 10^6$	680
B	87	1.4	5.8	.87	707
C	75	1.6	6.3	.79	638
D	50	1.4	6.3	.78	630
E	30	2.4	8.5	.72	581

It is obvious that the single-domain model does not describe the behavior of these specimens. In part, this may be due to use of a Lorentz internal field. For the more dilute specimens, however, the internal field correction is very small, and the particular choice of the internal field can have little influence. On the other hand, the strong tendency of these particles to agglomerate into clumps may make the internal field approach as such subject to question.

In an attempt to make the model more realistic, the properties of a slightly more sophisticated version have been studied. This work is far from complete, but it shows promise, and the results to date will be given here.

In this model, the particles are assumed to be uniaxial and grouped in clumps, and the clumps are assumed to interact through an internal field, here chosen as the Lorentz field. The purely magnetic work done in assembling the particles into their actual configuration in the applied magnetic field is

$$F = \sum_i k_i \sin^2 \phi_i - H_0 \sum_i m_i \cos \alpha_i - 1/2 \sum_i \vec{m}_i \cdot \left( \sum_{j \neq i} \vec{H}_{ij} \right)$$

where the sums are over all particles,  $k_i$  is the anisotropy constant, including magnetostriction, for the  $i$ th particle,  $\phi_i$  the angle between the particle magnetization vector and the particle easy axis,  $H_0$  the applied field (corrected for surface demagnetizing effects),  $\vec{m}_i$  the particle moment,  $\alpha_i$  the angle between the particle magnetization vector and the applied field, and  $\vec{H}_{ij}$  the magnetic field produced by the  $j$ th particle at the  $i$ th particle.

If the particles are grouped into clumps, and the clumps assumed to interact through a Lorentz field, then the last term may be divided by summing separately inside and outside the clumps:

$$\begin{aligned}\sum_{j \neq i} \vec{H}_{ij} &= \frac{4\pi I}{3} + \sum_{j \neq i}^* \vec{H}_{ij} \\ &= \frac{4\pi}{3} \sum_i m_i \cos \alpha_i + \sum_{j \neq i}^* \vec{H}_{ij}\end{aligned}$$

where  $\sum^*$  signifies that the sum is to be taken only over the particles in the same clump as the  $i$ th particle. The total work then becomes:

$$F = \sum_i k_i \sin^2 \phi_i - H_0 \sum_i m_i \cos \alpha_i - \frac{2\pi}{3} \left( \sum_i m_i \cos \alpha_i \right)^2 - 1/2 \sum_i \vec{m}_i \cdot \left( \sum_{j \neq i}^* \vec{H}_{ij} \right)$$

The variable coordinates involved are the angles defining the magnetization vectors within the framework of their crystal axes. The determination of the values of these coordinates, which should determine the macroscopic magnetization vs. field strength relation, is then a problem in determining the values that minimize this work.

In order to solve this problem, further simplifying assumptions must be made. The moments and anisotropy constants are assumed to be the same for all particles. Furthermore, specific configurations must be assumed for the clumps, and the interaction of the particles within the clump calculated explicitly. This latter is the truly involved part of the calculation. As a start, the simplest possible clump consisting of two spherical particles, was chosen. Further, it was assumed that their easy axes coincided, since this would be the position of minimum energy in the absence of an external field. The magnetic interaction was accounted for by considering each particle to behave magnetically as an ideal dipole placed at the center of the particle.

A completely detailed calculation of the magnetization curve of a random collection of such clumps would involve numerical integration of the clump magnetization curves over all angles of orientation of the easy axes with respect to the field direction. This has not been completed.

Consideration of the qualitative aspects of the model has shown some correspondence with the data given above for the Fe-85 specimens, however.

The interaction term for this type of clump is

$$\frac{1}{2} \sum_i \vec{m}_i \cdot \sum_{i \neq j}^* \vec{H}_{ij} = \frac{1}{2} (\vec{m}_1 \cdot \vec{H}_{12} + \vec{m}_2 \cdot \vec{H}_{21}) = \vec{m}_1 \cdot \vec{H}_{12}$$

because of the symmetry of the magnetic energy expressions. Referring to Figure 3-8, this becomes

$$\begin{aligned} \vec{m}_1 \cdot \vec{H}_{12} &= \frac{3(\vec{m}_1 \cdot \vec{r}_{12})(\vec{m}_2 \cdot \vec{r}_{12})}{r_{12}^5} - \frac{\vec{m}_1 \cdot \vec{m}_2}{r_{12}^3} \\ &= \frac{m^2}{r^3} \left\{ 2 \cos \phi_1 \cos \phi_2 - \sin \phi_1 \sin \phi_2 \cos(\psi_1 - \psi_2) \right\} \end{aligned}$$

Further,  $\cos \alpha_1$  may be expressed as

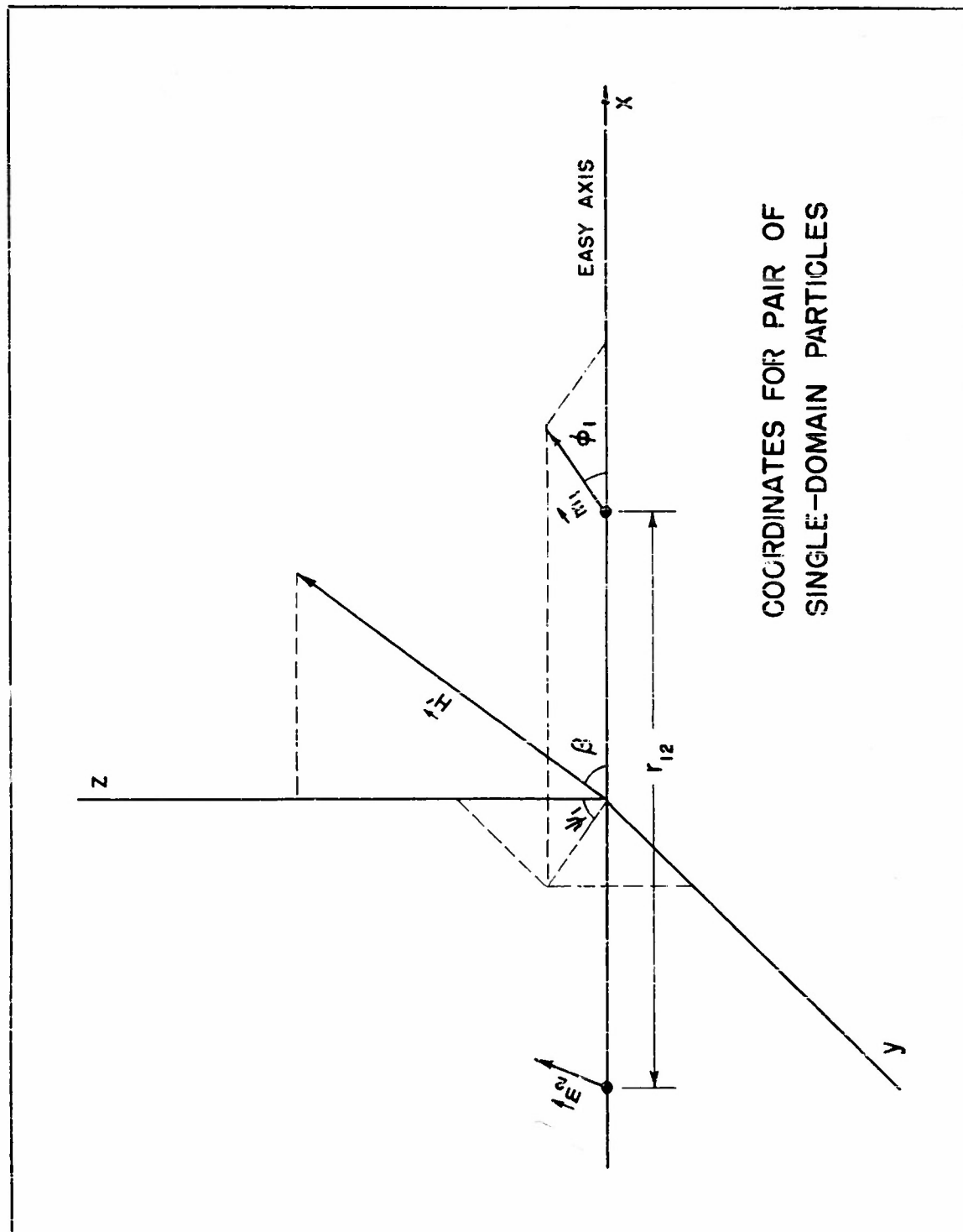
$$\cos \alpha_1 = \sin \phi_1 \cos \psi_1 \sin \beta + \cos \phi_1 \cos \beta$$

Then for a given value of  $\beta$ , the minimization equations become

$$(3.1) \quad \frac{\partial F}{\partial \phi_1} = k \sin 2 \phi_1 - H^* m (\cos \phi_1 \cos \psi_1 \sin \beta - \sin \phi_1 \cos \beta) + \frac{m^2}{r^3} \left\{ 2 \sin \phi_1 \cos \phi_2 + \cos \phi_1 \sin \phi_2 \cos(\psi_1 - \psi_2) \right\} = 0$$

$$(3.2) \quad \frac{\partial F}{\partial \psi_1} = H^* m \sin \phi_1 \sin \psi_1 \sin \beta - \frac{m^2}{r^3} \sin \phi_1 \sin \phi_2 \sin(\psi_1 - \psi_2) = 0$$

The equations in  $\phi_2$  and  $\psi_2$  are symmetrical with these. This symmetry suggests that in any solution,  $\phi_1 = \phi_2 = \phi$ , and  $\psi_1 = -\psi_2 = \psi$ . Physically, this means that both dipoles will make the same angle with respect to the easy axes, and will arrange themselves symmetrically on either side of the plane containing  $H^*$  and the common easy axis.



An insight into the behavior of this model may be gained by considering special cases.

Case (1):  $\beta = \pi$   $\sin \beta = 0$ ;  $\cos \beta = -1$

The field  $H^*$  is then directed along the easy axis, in the opposite direction to the magnetization vectors when  $\phi = 0$ . Equation (3.2) becomes

$$\frac{\partial F}{\partial \psi} = 0 = -\frac{m^2}{r^3} \sin^2 \phi \sin 2\psi$$

There are two possible solutions to this equation

- a)  $\sin \phi = 0$
- b)  $\sin \phi \neq 0$ ,  $\sin 2\psi = 0$

In the second case, the extremum defined by the solution will be a minimum as long as

$$\frac{\partial^2 F}{\partial \psi^2} = -\frac{2m^2}{r^3} \sin^2 \phi \cos 2\psi > 0$$

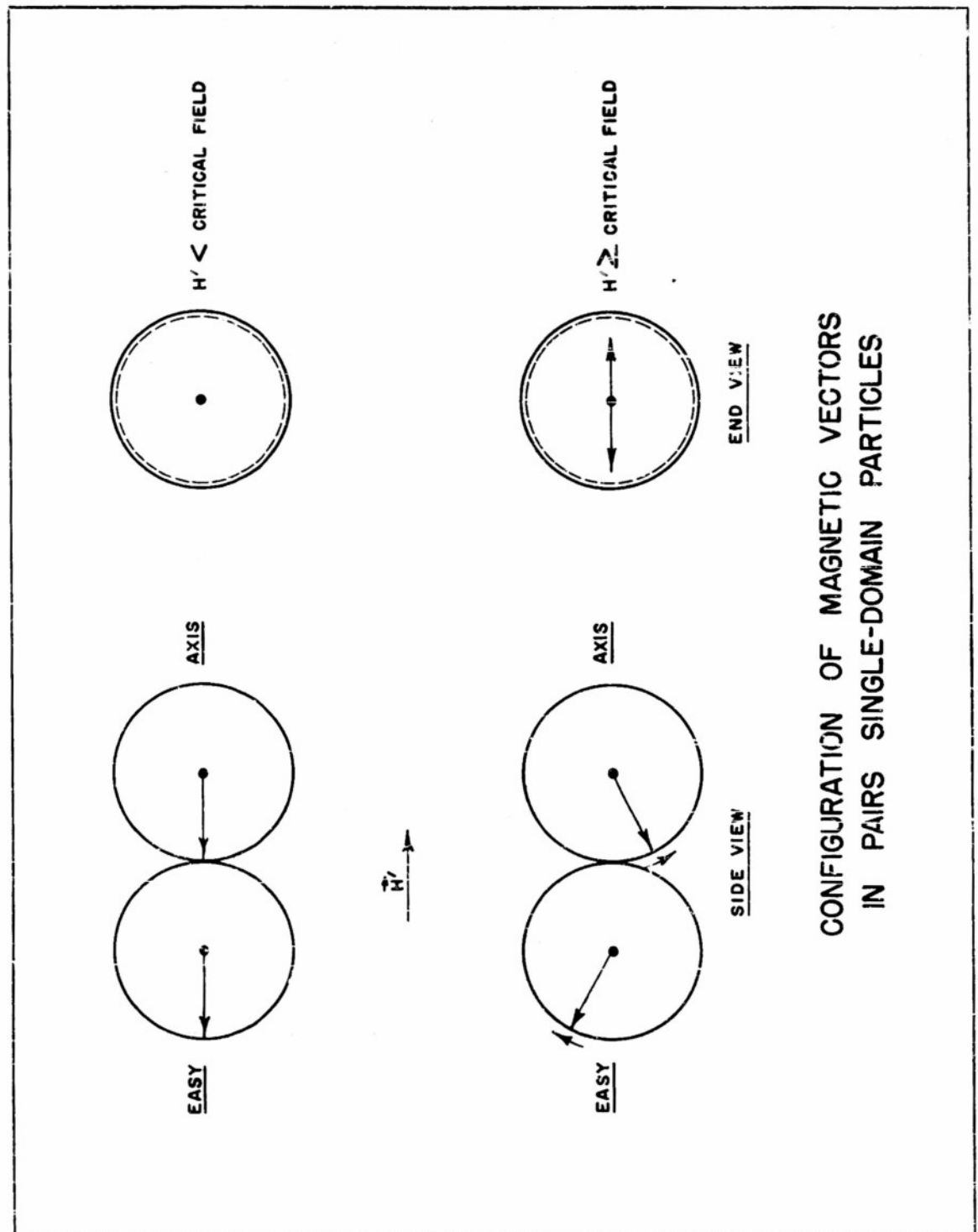
Both conditions together imply  $\psi = \pi/2$ . Therefore, when the magnetization vectors do leave the easy axis ( $\sin \phi$  becomes  $> 0$ ), they will do so in a common plane, as illustrated in Figure 3-9. It can be shown that equations (3.1) and (3.2) will be correct if  $\cos 2\psi$  is set  $= -1$  for the case of  $\sin \phi = 0$ , as well.

Returning to equation (3.1), the equilibrium value for  $\phi$  may be obtained, using  $\sin \beta = 0$ ,  $\cos \beta = -1$  and  $\cos 2\psi = -1$

$$\frac{\partial F}{\partial \phi} = 0 = K \sin 2\phi - H^* m \sin \phi + \frac{m^2}{2r^3} \sin 2\phi$$

collecting:

$$\left(k + \frac{m^2}{2r^3}\right) \sin 2\phi = H^* m \sin \phi$$



CONFIGURATION OF MAGNETIC VECTORS  
IN PAIRS SINGLE-DOMAIN PARTICLES

This is identical to the minimization of energy for a single-domain particle<sup>(9)</sup> with the field directed along the easy axis. Thus for this case, the clump behaves like a single-domain particle whose anisotropy constant is given by

$$k' = k + \frac{m^2}{2r^3}$$

Case 2:  $\beta = \pi/2$      $\sin \beta = 1$      $\cos \beta = 0$

The field is then directed perpendicular to the mutual easy axis. Equation (3.2) becomes:

$$(3.3) \quad \frac{\partial F}{\partial \psi} = H'm \sin \phi \sin \psi - \frac{m^2}{r^3} \sin^2 \phi \sin 2\psi = 0$$

A possible solution is  $\sin \psi = 0$ ,  $\cos \psi = 1$ ,  $\psi = 0$ . This represents a minimum when:

$$\frac{\partial^2 F}{\partial \psi^2} = H'm \sin \phi \cos \psi - \frac{2m^2}{r^3} \sin^2 \phi \cos 2\psi > 0$$

(3.4) or  $H' > \frac{2m \sin \phi}{r^3}$

Equation (3.1) becomes, using this solution for  $\psi$

$$\frac{\partial F}{\partial \phi} = k \sin 2\phi - H'm \cos \phi + \frac{3m^2}{2r^3} \sin 2\phi = 0$$

(3.5) or  $\left(k + \frac{3m^2}{2r^3}\right) \sin 2\phi = H'm \cos \phi$

This is the energy minimization equation for a single-domain particle in a field perpendicular to the easy axis. One solution is:

$$\cos \phi = 0 \quad \phi = \pi/2$$

The second derivative becomes

$$(3.6) \quad \frac{\partial^2 F}{\partial \phi^2} = 2 k'' \cos 2\phi + H'm \sin \phi$$

$$= H'm - 2k''$$

$$\text{Where } k'' = k + \frac{3m^2}{2r^3}$$

This is positive only when

$$H' > \frac{2k''}{m} = \frac{2k + \frac{3m^2}{r^3}}{m}$$

For these fields, the condition of equation (3.4) holds, so that  $\psi = 0$  is the proper solution of equation (3.3). A second solution for equation (3.5) is

$$\sin \phi = \frac{H'm}{2k''}$$

The second derivative is then

$$\frac{\partial^2 F}{\partial \phi^2} = 2k'' (1 - 2 \sin^2 \phi) + H'm \sin \phi > 0$$

$$H' < \frac{2k''}{m}$$

For fields less than this upper limit, the condition of equation (3.4) then becomes

$$H' > \frac{2m \sin \phi}{r^3} = \frac{H'm^2/r^3}{k + 3m^2/2r^3}$$

which is always fulfilled. Therefore, over the entire range of field strength, the proper solution for equation (3.3) is  $\psi = 0$ . The magnetic moments of the two particles of the clump move together, both in the

plane defined by the applied field and the common easy axis.

The overall behavior in this case is that of a single-domain particle with anisotropy constant  $k'' = k + \frac{3m^2}{2r^3}$ . Furthermore, it can be shown by a similar analysis that this result holds for all values of  $\beta$  from 0 to  $\pi/2$ .

Case (2) corresponds to the situation for all clumps in the region of the approach to saturation. Therefore, the anisotropy constant per particle of this model calculated from the approach to saturation should be

$$k_2 = k + \frac{3m^2}{2r^3}$$

For the initial slope of the magnetization, at least some of the clumps will correspond to Case (1), in which the effective field lies along the easy axis, directed against the particle moments, while some will correspond to Case (2). The anisotropy constant calculated from the initial slope should therefore lie between that for cases (1) and (2)

$$k_2 = k + \frac{3m^2}{2r^3} > k_1 > k + \frac{m^2}{2r^3}$$

Inspection of the data in Table 3-4 shows that in every case  $k_2 > k_1$ . The analysis was not carried beyond this point; the conclusions must be limited to the observation that while a simple single-domain model does not fit the data, allowing for the formation of clumps appears to show promise in explaining certain features of the data.

### 3.2.3 Mixtures of High and Low Coercive Force Powders

In order to study the effect upon the magnetic properties of compacts of mixed materials of widely different intrinsic properties, a series of mixtures was prepared consisting of varying proportions of a

THE FRANKLIN INSTITUTE • Laboratories for Research and Development  
F-2236

5-micron carbonyl Fe (General Aniline and Film Corp. "HP") and powdered "Ferroxdure", obtained through the courtesy of the Ferroxcube Corp. This material is a permanent magnet oxide whose nominal composition is  $\text{BaFe}_{12}\text{O}_{19}$ . For this experiment, a solid piece of the ceramic was ball-milled until the particles were of the order of 0.1 to 2 microns in diameter. This was mixed with the appropriate amount of "HP" and ball-milled in a dilute solution of Duco cement in acetone. Compacts  $1/4$  in. x  $1/4$  in. x 1 in. were pressed at 12 tsi. The magnetic measurements were made in the Sanford-Bennett<sup>(11)</sup> permeameter.

The magnetic properties of these specimens are summarized in Table 3-6.

TABLE 3-6

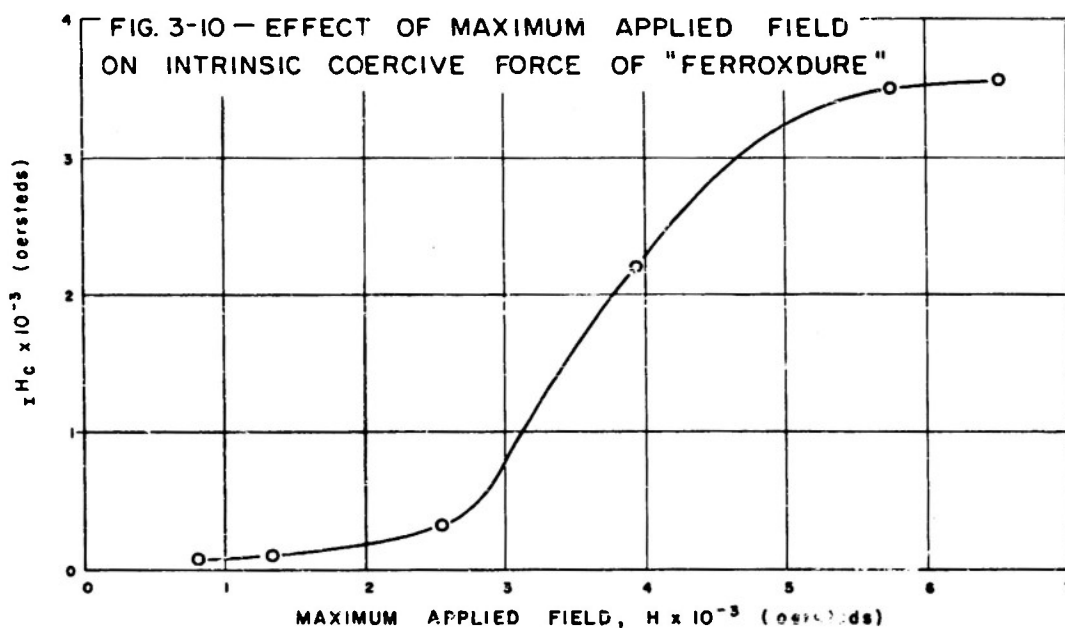
Magnetic Properties of Ferroxdure-"HP" Compacts

Wt % "HP"	Density	$4\pi I_s$	$4\pi I_r$	$I^H_c$
100	5.21 g/cm <sup>3</sup>	14130 gaussess	380 $\pm$ 100 gaussess	11 Oe
83	4.89	11350	929	84
62	4.57	9100	1550	248
35	4.03	5800	1445	800
0	3.72	3100	1450	2850

The saturation magnetizations were calculated by plotting  $4\pi I$  as a function of  $H^{-1}$  in the region of field strengths from 2000 to 7000 Oe, and extrapolating to infinite field strength. For the compacts containing either "HP" or Ferroxdure alone, the saturation moment per gram of the separate substance could be calculated. These values are:

	<u>Observed</u>	<u>Literature</u>
"HP"	216 emu/g	217.8 <sup>(2)</sup> emu/g
Ferroxdure	66	70 <sup>(15)</sup>

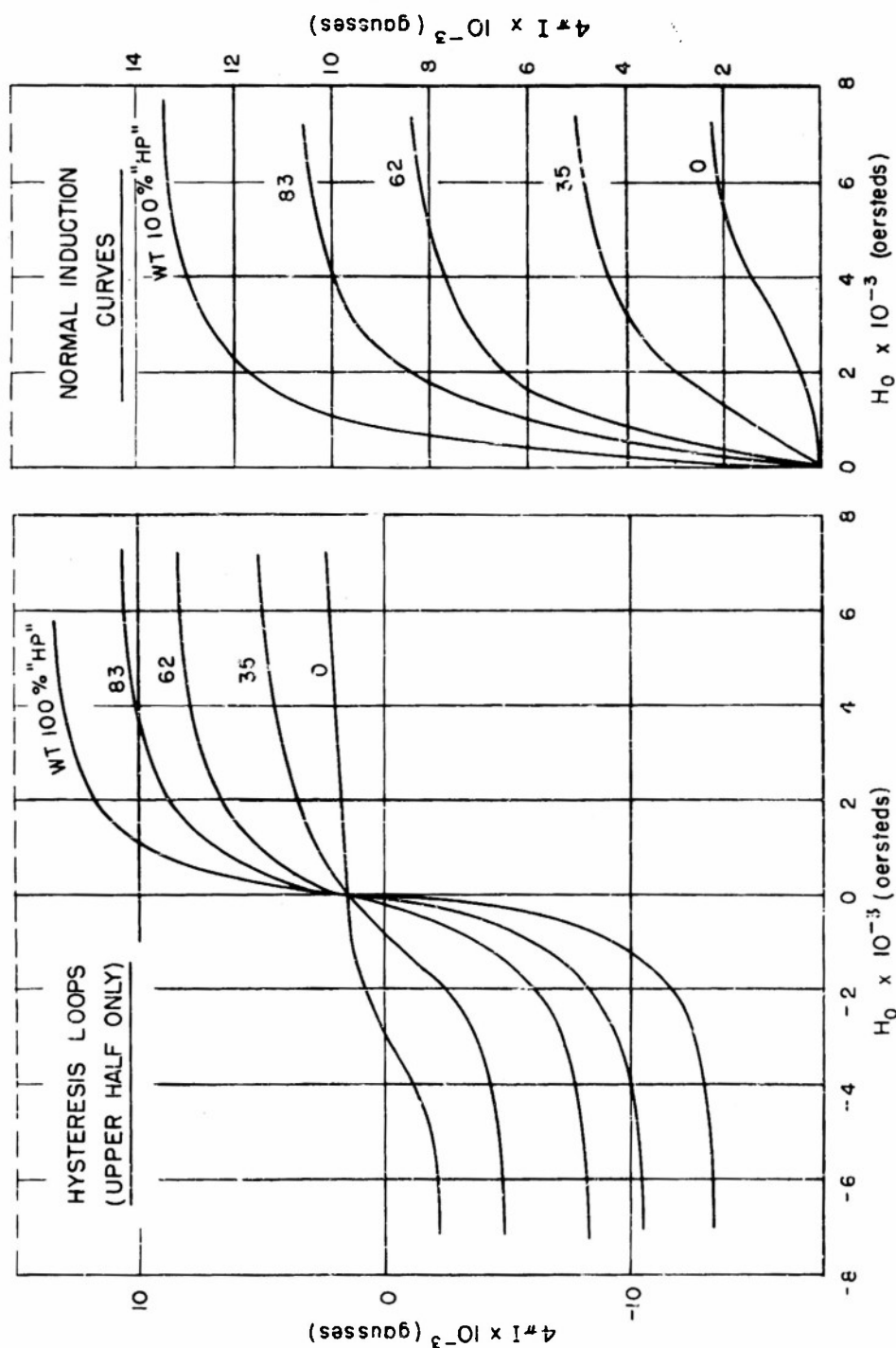
The Ferroxdure was not completely saturated in the field strengths available here. Figure 3-10 shows the coercive force as a function of the maximum field strength applied to the sample. The maximum attainable



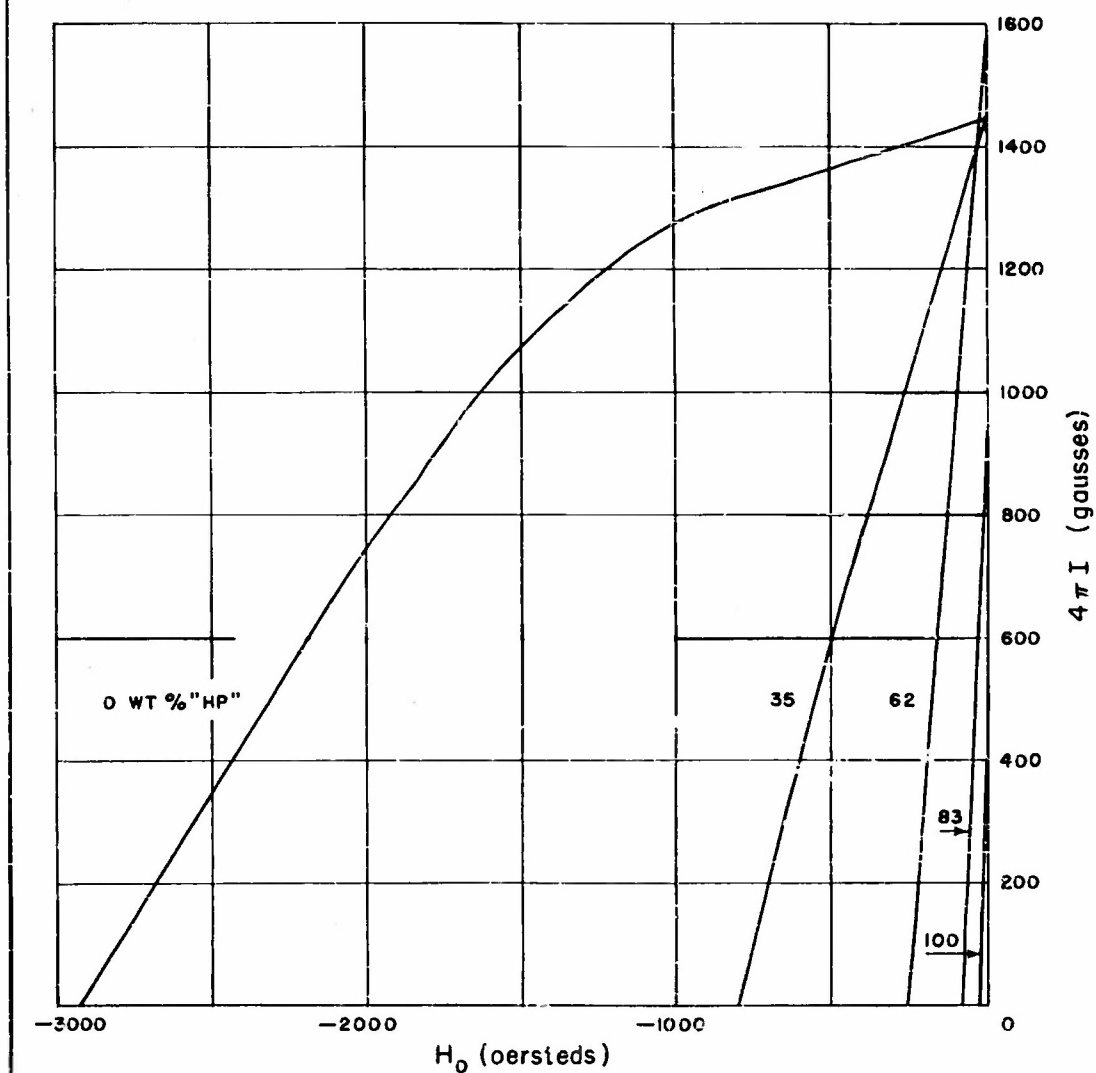
coercive force has not been reached. The extrapolation to saturation is thus much worse than in the case of "HP", which probably accounts for the low observed moment/g.

Figure 3-11 shows the normal induction curves and hysteresis loops of these specimens. In Figure 3-12, the demagnetizing portions are shown in greater detail. The outstanding characteristic of these curves is the sharp reduction in coercive force that occurs with a small addition of "HP". At 35% "HP" by weight (25% by volume), the intrinsic coercive force drops from 2850 to 800 Oe. At the same time the shape of the hysteresis loop changes radically. The shoulder in the demagnetizing portion disappears, and the normal induction curve no

# MAGNETIC PROPERTIES OF FERROXDURE "HP" COMPACTS



# DEMAGNETIZING CURVES OF FERROXDURE - "HP" COMPACTS



REPORT F-2236

FIGURE 3-12

longer exhibits a point of inflection. The remanent magnetization, on the other hand, stays high up to 50% "HP" by volume, and then drops rapidly. This drastic effect upon the coercive force of the presence of low-coercive material is in line with the results of Meiklejohn<sup>(16)</sup> on mixtures of Fe powders, and points up the importance of taking into account the interaction between the particles in interpreting the behavior of these materials.

### 3.3 Effect of Degree of Reduction on Magnetic Properties of Single-Domain Particles

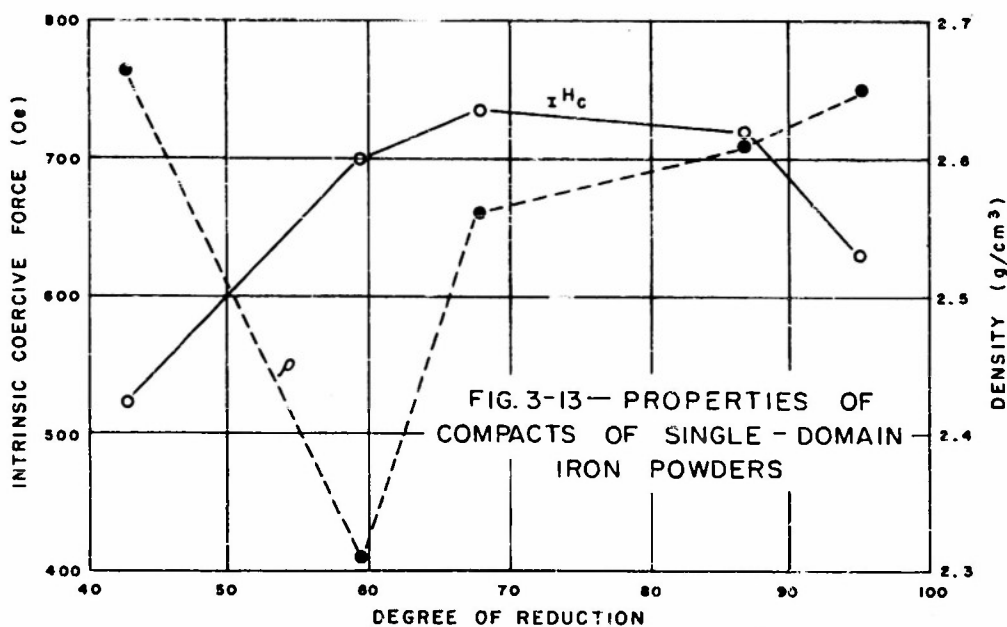
In Progress Report F-2236-10, it was pointed out that for a series of powders of roughly the same particle size, but of varying degrees of reduction, the intrinsic coercive force did not appear to depend markedly upon the degree of reduction. Because of the sensitivity of the coercive force to particle size it is important to maintain the same particle size in such a comparison. This experiment has therefore been repeated, taking greater care to maintain the same size. Degrees of reduction were measured by hydrogen evolution, and correspond to weight percent of free Fe present in the specimen. Pressed (12 tsi) bars were prepared, using Duco cement as a binder, having dimensions 1/4 in x 1/4 in x 1 in. The magnetic measurements were made using the Sanford-Bennett<sup>(11)</sup> permeameter. The data is given in Table 3-7.

TABLE 3-7

#### Magnetic Properties of Partially Reduced Fe Powders

Sample	Particle Diameter	% Red.	( $I^H_c$ )	Density
Fe-115	187 $\text{\AA}$	42.9	521 Oe	2.66 g/cm <sup>3</sup>
Fe-116	174	59.6	699	2.31
Fe-121	165	68.0	734	2.56
Fe-120	190	87.0	721	2.61
Fe-122	182	95.0	630	2.65

In Table 3-7, the first column gives the sample designation, the second the particle diameter measured using Warren's<sup>(17)</sup> simple technique on x-ray diffraction line broadening (see Quarterly Report P-2236-8), the third the degree of reduction, the fourth the intrinsic coercive force, and the fifth the densities of the compacts. The intrinsic coercive force and the density is plotted in Figure 3-13 against the degree of



reduction. The maximum coercive force occurs near 70% reduction. This measured coercive force is dependent to some extent upon pressing conditions, however. Although all specimens were given identical pressing treatments, the densities vary quite widely. This variation may be due to accidental differences in pressing, or to real differences in pressing characteristics. At best, it can be said as a practical matter that under identical conditions, a small maximum in the coercive force appears at about 70% reduction. Lith<sup>(18)</sup> found a maximum at about 65%, although

in his work no attempt was made to keep the Fe particle size uniform.

The degree of reduction seems to have only a slight effect on the coercive force; on the other hand, reoxidation has been observed to have a drastic effect, although this has not been put on a quantitative basis. Storage of these powders under commercially-obtained benzene or acetone for as little as several weeks resulted in a large decrease in free-metal content and in magnetic properties. By adding a small amount of  $\text{CaH}_2$  to the benzene storage bottle, however, the benzene could be dried very effectively, and the reoxidation apparently stopped. Under these conditions, the powders have been stored for periods up to several months without appreciable change.

Reoxidation also occurs with the powders in the form of pressed compacts, even when about 70% by Wt % Duco has been added before pressing. Adequate protection, however, could be given the compacts if, immediately after forming, they were evacuated and then covered with a solution 4 Wt % of Acryloid\* in acetone, so that the compact is impregnated by the resin. Table 3-8 shows the results of tests on impregnated and unimpregnated specimens.

TABLE 3-8

## Reoxidation of Single-Domain Fe Compacts

Material	Date	$I^H_c$	$4\pi I_r$	$4\pi I_s$	Impregnated
Fe-105	9-30-53	545	2047	5004	No
	1-18-54	519	2020	5025	
Fe-106	9-30-53	441	817	2755	No
	1-18-54	349	800	2660	
Fe-104	10-30-53	171	1142	5043	Yes
	1-18-54	170	1176	5029	
Fe-107	11-2-53	401	1538	4560	Yes
	1-18-54	394	1515	4523	

---

\* Thermoplastic resin, Rohm and Haas Company

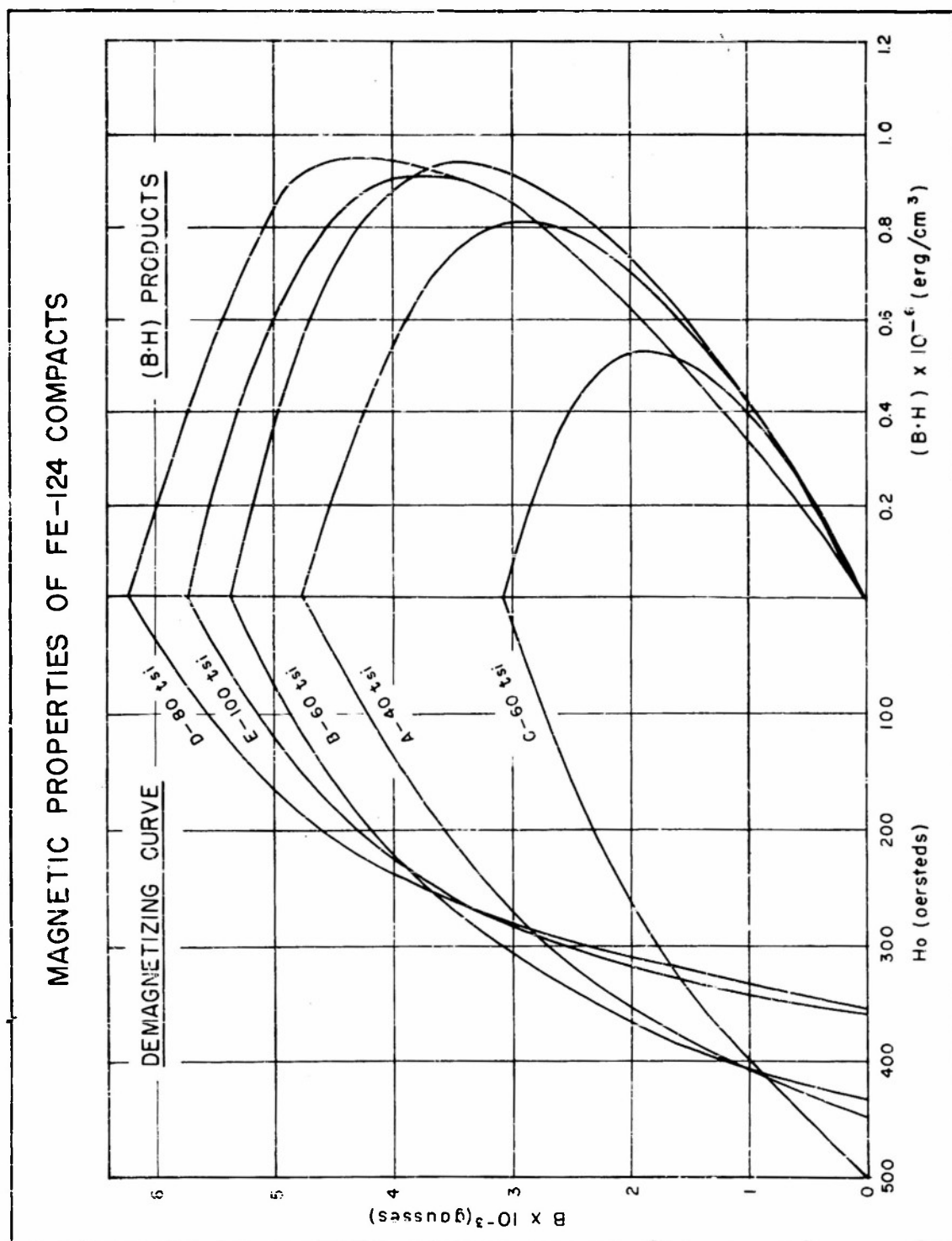
Reoxidation affected the coercive force most strongly. It was almost completely inhibited by the impregnation.

### 3.4 Permanent Magnet Properties of Fe Powders

While no direct attempt was made during this work to achieve high  $(BH)_{\max}$  values, from time to time promising powders were pressed at a variety of pressures to check their permanent magnet properties. The result of such an experiment was reported in Progress Report P-2236-11. The moment per gram of those specimens, expressed as  $4\pi I_g/\rho$ , was of the order of 1840 gauss  $\text{cm}^3/\text{g}$ , as compared to 2730 for bulk Fe. This low value must have been due to reoxidation of the specimens during preparation, and was attended by a low  $(BH)_{\max}$  of about  $0.45 \times 10^6$  ergs/ $\text{cm}^3$ . The powder itself was originally 80% by weight free metal, which should have resulted in  $4\pi I_g/\rho$ , no less than 2180 gauss- $\text{cm}^3/\text{g}$ , but chemical analysis showed a drop to 60% by weight free metal, corresponding to  $4\pi I_g/\rho$  of no less than 1640 gauss- $\text{cm}^3/\text{g}$ . A similar experiment was run subsequently. Fe-124, which analyzed to 85% by weight free Fe and possessed an x-ray diameter of 171 Å, was pressed into bars 1 1/4 in. x 1/8 in. x about 1/16 in. at pressures from 40 to 100 tsi. The pressing was done by the group at Lehigh University under Professor Joseph Libsch. The powder before pressing and the compacts after were kept under benzene dried with  $\text{CaH}_2$ . The magnetic properties are summarized in Table 3-9, and the demagnetizing portions of the B-H curves are shown in Figure 3-14.

TABLE 3-9  
Magnetic Properties of Fe-124 Compacts

Specimen	Pressure tsi	$4 \pi I_s$ gauss	$4 \pi I_r$ gauss	$H_c$ Oersted	$(BH)_{\max}$ ergs/cm <sup>3</sup>	$\rho$ g/cm <sup>3</sup>	$4 \pi I_g/\rho$ gauss cm <sup>3</sup> /g	$I_r/I_s$
Fe-124-A	40	8,144	4,750	447	$.83 \times 10^6$	3.308	2460	.58
B	60	9,239	5380	434	.93	3.985	2320	.58
C	60	5,760	3080	500	.53	3.128	1840	.54
D	80	10,020	6220	355	.95	4.05	2475	.62
E	100	8,941	5730	358	.92	4.075	2195	.64



REPORT F-2236

FIGURE 3-14

Specimen Fe-124-C became quite hot during pressing, indicating that considerable reoxidation took place. Its properties are close to those in the previous experiment discussed above. The other specimens all exhibit considerably higher values of  $4\pi I_s/p$ , lower coercive forces, and higher densities. Apparently, in conformity to the suggestion of Lihl<sup>(18)</sup>, the oxide layer imposes a minimum closeness of approach of the dominant Fe cores of the particles. This enforced separation results in a high coercive force and a low saturation magnetization. The maximum  $(BH)_{\max}$  value,  $0.95 \times 10^6$  ergs/cm<sup>2</sup>, is found for the material that is apparently the least oxidized, Specimen D. This maximum value is associated with a rather low coercive force, 355 Oe, but a high remanence to saturation ratio. This ratio, for non-interacting, randomly oriented single domain particles, should be  $\sim 0.5$ <sup>(9)</sup>. It seems probable that particle interaction should tend to reduce the ratio since the magnetized state must represent a lower entropy state than the demagnetized, and particle interactions should provide the high, local fields necessary to allow domain orientations to assume more or less random distributions. It is probable, therefore, that a preferred direction exists within the compacts and coincides with the direction of measurement.

As a working hypothesis, the following is suggested. For the powders without an oxide layer, a certain amount of effective particle growth can take place under the influence of the pressure. This occurs in such a way as to introduce a slightly preferred direction, magnetically speaking, and a lower coercive force because of the effective particle size increase.

The  $(BH)_{\max}$  value noted here,  $0.95 \times 10^6$  ergs/cm<sup>3</sup>, is not especially high. French workers<sup>(19)</sup> have reported the following:

Material	Density g/cm <sup>3</sup>	B <sup>H</sup> <sub>c</sub> Oersteds	4πI <sub>r</sub> Gauss	(BH) <sub>max</sub> ergs/cm <sup>3</sup>
Formate Fe	6.5	410	5700	1.0 x 10 <sup>6</sup>
"		400	5500	.95
" + 1% CaO		550	5600	1.37
" "		425	6500	1.19

The value of (BH)<sub>max</sub> reported here about matches the best observed for pure Fe. This has been achieved in this case with a higher remanence and a lower coercive force than in the French case. Considerably higher (BH)<sub>max</sub> values are noted for the powders produced with unreducible oxides added. In this table, these (BH)<sub>max</sub> values were calculated by assuming that the ratio (BH)<sub>max</sub>/B<sub>r</sub>H<sub>c</sub> is the same, 0.43, as for our Specimen Fe-124D. The highest value noted above, 1.37 x 10<sup>6</sup>, agrees with the value of 1.36 x 10<sup>6</sup> given by Weil<sup>(20)</sup> as the best produced with Fe powders. The remanence of the French magnets was of the same order as in our specimen Fe-124-D, but the coercive forces were higher. This increase in coercive force produces the increase in (BH)<sub>max</sub> values.

The hypothesis discussed above, together with these observations, suggests that in order to attain the maximum (BH)<sub>max</sub>, the powder chosen should, if it is pure Fe, possess a particle size slightly smaller than that corresponding to the maximum coercive force in the loosely compacted state. Particle growth occurring during pressing should then not have so drastic an effect on the coercive force.

### 3.5 Alloy Powders

The high coercive forces expected of single domain ferromagnetic powders are considered<sup>(21)</sup> to arise from magnetocrystalline anisotropy, shape anisotropy, or magnetostriction and stress. Of these, the first should be the easiest to control, since it depends only on the crystal

phase present. During the course of this program, some experiments were conducted with two alloys expected to have high magneto-crystalline anisotropies.

The first of these, the alloy whose composition is FePt, has been reported<sup>(22)</sup> to possess a tetragonal ordered phase, where high anisotropy might be expected. Weil<sup>(23)</sup> has reported intrinsic coercive forces as high as 10,000 oersteds for fine powders of this alloy. Work here progressed only to the point of showing that fine powders of approximately the right composition and crystal phase can be produced by reduction of FePtCl<sub>6</sub>.

The second alloy considered was that of composition FeBe<sub>2</sub>. The magnetic data available in the literature indicate that reasonably interesting magnetic properties should be exhibited by single-domain particles. Table 3-10 contains these expected properties.

TABLE 3-10

Expected Magnetic Properties of Single-Domain FeBe<sub>2</sub> Powders

Property	Value	Reference
X-ray Density	4.6 g/cm <sup>3</sup>	24
Saturation Moment per gram	169.3 cgs	25
Saturation Volume Magnetization	785 gauss	a
Magnetocrystalline Anisotropy	$K_1 = 1.7 \times 10^6$ ergs/cm <sup>3</sup>	b
Curie Temperature	643°C	25
Domain Wall Energy	219 ergs/cm <sup>2</sup>	c

TABLE 3-10 (cont)

Expected Magnetic Properties of Single-Domain FeBe<sub>2</sub> Powders

Property	Value	Reference
Critical Radius for Single Domain Particles	336 Å	d
Maximum Intrinsic Coercive Force for Spheres	4330 Oe	e
Maximum Remanence	4930 Gauss	e
Crystal Lattice	MgZn <sub>2</sub> Type	24
	a = 4.212 Å	24
	c = 6.834 Å	24
	d = 2.57 Å = Ave. Fe-Fe Separation	24

## NOTES:

- a. The saturation volume magnetization was calculated from the x-ray density and the saturation moment per gram.
- b. The magnetocrystalline anisotropy constant was estimated from the approach to saturation data. Meyer and Taglang<sup>(25)</sup> plotted  $I$  vs  $H^{-1}$ , and obtained as a value for  $A$ , the coefficient of magnetic hardness, in the equation

$$I = I_0 \left(1 - \frac{A}{H}\right)$$

$$A = 415 \text{ Oe}$$

Cobalt shows a value of about 1000. Assuming these values are in the

## NOTES (cont)

same ratio as the anisotropy constants, and using  $K_1 = 4.1 \times 10^6$  ergs/cm<sup>3</sup>(2) for Co, the value of  $K_1$  for FeBe<sub>2</sub> in the table was calculated. This is only a very crude estimate.

- c. Kittel<sup>(21)</sup> gives for the wall energy of a domain

$$\sigma_w = \left[ \frac{kT_c K_1}{d} \right]^{1/2}$$

The estimated anisotropy constant  $K_1$  given above and the values for the Curie point  $T_c$  and the Fe-Fe separation  $d$  given in the table were used in this calculation.

- d. For the critical radius for high anisotropy uniaxial crystals, Kittel<sup>(21)</sup> gives

$$R_c = \frac{9 \gamma_w}{4 \pi I_s^2}$$

- e. For non-interacting uniaxial single-domain particles, the maximum intrinsic coercive force is expected to be<sup>(9)</sup>

$$I_c^H = \frac{2K_1}{I_s}$$

and the maximum remanence<sup>(9)</sup>

$$I_r = 0.5 I_s$$

FeBe<sub>2</sub> is a derinite phase ( $\epsilon$ -phase) with a congruent melting point at 1480°C<sup>(26)</sup>. Melts were prepared of this phase in a straightforward fashion. The composition and homogeneity were checked by standard chemical techniques. X-ray patterns showed only the desired phase. The sample chosen for further study analyzed to 70.4 to 71.3 Wt % Fe,

or 27.8 to 28.6 at % Fe. This is well within the  $\epsilon$ -phase region<sup>(26)</sup>. The material was ground in a Plattner mortar, and screened through a 325 mesh screen. This was then further fractionated by settling through a vertical column of benzene in the center of a vertical solenoid. The fractions dropping out at various field strengths were collected, and the magnetic properties measured in loose powder form in the permeameter.

The x-ray patterns of these finely divided powders still showed only the desired  $\epsilon$ -phase<sup>(26)</sup>. No line broadening was observed, indicating the crystallites were  $> 1000 \text{ \AA}$  in diameter. Electron micrograph particle size counts of the fractions were made. Table 3-11 summarizes the data on these fractions.

TABLE 3-11

Specimen	Properties of $\text{FeBe}_2$ Powders				
	$\bar{d}$ microns	$4\pi I_s$ Gausses	$4\pi I_r$ Gausses	$I_H$ Oersteds	$I_r/I_s$
C- $\text{FeBe}_2$ -4-1	3.1	1173	124	48	.11
C- $\text{FeBe}_2$ -4-2	3.2	1463	100	44	.07
C- $\text{FeBe}_2$ -4-3	2.7	1780	196	53	.11
C- $\text{FeBe}_2$ -4-4	1.8	1787	155	48	.09
C- $\text{FeBe}_2$ -4-4.4	.4	2278	505	68	.22

In the table,  $\bar{d}$  is the number average particle size, determined from counts of electron micrographs. The distributions were quite broad, and too much significance cannot be attributed to the quoted sizes. It is obvious that the single-domain size was not reached. The ratio  $I_r/I_s$ , which exceeds 0.5 in single domain Fe, was never above 0.22. Regrinding of the finest powder produced no essential change in its magnetic properties. Apparently the lower limiting particle size attainable by grinding had been reached.

It was proposed to produce  $\text{FeBe}_2$  powder by reduction of  $\text{Be}_2\text{Fe}(\text{CN})_6$ . This was precipitated from a mixture of  $\text{BeCl}_2$  and  $\text{K}_4\text{Fe}(\text{CN})_6$  solutions in a straightforward way. Preliminary experiments showed that no simple thermal decomposition occurred with this compound as it did with ferrous formate. Reduction with  $\text{CaH}_2$  indeed produced a fine ferromagnetic powder, but it contained considerable  $\alpha\text{-Fe}$ . The experiments were not carried beyond this point.

#### 4. SUMMARY

The work of this program, over the three years of its existence, has been mainly that of determining clearly the factors controlling the particle size, and perhaps shape, of Fe particles produced by reduction from oxides. The oxide produced by thermal decomposition of ferrous formate was shown to be basically  $\text{Fe}_3\text{O}_4$ , with considerable metallic Fe present. When the oxide crystallites are of the order of several hundred angstrom units across, each oxide crystallite produces one Fe particle during low temperature reduction.

By selecting the appropriate particle size, produced under completely controlled conditions, reasonably high  $(\text{BH})_{\text{max}}$  values, of the order of  $0.95 \times 10^6 \text{ ergs/cm}^3$ , were obtained in compacts of these Fe powders. The evidence indicates that the highest values should be obtained by selecting particles whose dimensions are somewhat smaller than those possessing the maximum coercive force in the loose powder. For these particles, agglomeration under pressure should tend to increase the coercive force slightly rather than reduce it. It is important to prevent reoxidation in order to obtain the best magnetic properties.

The magnetic behavior of compacts of these single-domain particles does not fit the theory given for non-interacting single-domain particles. It has been shown that the discrepancies observed between theory and experiment are probably due to local interactions between particles within

THE FRANKLIN INSTITUTE • *Laboratories for Research and Development*

F-2236

clumps. These interactions might be understood by considering simple configurations of the particles in clumps, and extracting general types of behavior from these configurations. A start was made upon this, but it is too early to judge the success of this approach.

$\text{FeBe}_2$  is an alloy showing promise of interesting properties in single-domain particle form. Rough calculations indicate a critical diameter of about  $350 \text{ \AA}$  for single-domain particles. For particles with diameters down to about  $4000 \text{ \AA}$ , prepared by grinding, the coercive force increases slightly with decreasing particle size, but the single-domain region has not been reached at this writing.

Alan D. Franklin

Alan D. Franklin  
Project Leader

References

1. F. Lihl, *Monatsh. für Chemie* 81 632 (1950)
2. R. Bozorth, "Ferromagnetism", p. 242, Van Nostrand (1951)
3. E. J. W. Verwey, *Nature* 144 327 (1939)  
E. J. W. Verwey and P. W. Haayman, *Physica* 8 979 (1941)
4. R. W. G. Wyckoff, "The Structure of Crystals", 2d ed, Chemical Catalog Co., N. Y. (1931)
5. L. Neel, *Annales des Physique* 3 137 (1948)
6. L. Neel, *J. Phys. Radium* 5, 241 (1944)
7. H. Lawton and K. H. Stewart, *Proc. Roy. Soc.* 193A 72 (1948);  
*Proc. Phys. Soc.* 63A 848 (1950)
8. L. Neel, *J. Phys. Radium* 9 193 (1948)
9. T. Hostein and H. Primakoff, *Phys. Rev.* 59 388 (1941)
10. E. Stoner and E. Wohlfarth, *Phil. Trans. Roy. Soc.* 240A 599 (1948)
11. R. L. Sanford and E. Bennett, *J. Res. Nat. Bur. Std.* 10 567 (1933)
12. L. Néel, *Compt. Rend.* 224 1550 (1947)
13. L. Weil, *Compt. Rend.* 225 229 (1947)
14. R. Becker and W. Döring, "Ferromagnetismus" J. Springer, Berlin (1939)
15. J. J. Went, G. W. Rathenau, E. W. Gorter and G. W. van Oosterhout, *Philips Tech. Rev.* 13 194 (1952)
16. W. H. Meiklejohn, *Rev. Mod. Phys.* 25 302 (1953)
17. B. E. Warren, *J. Appl. Phys.* 12 375 (1941)
18. F. Lihl, *Acta Physica Austriaca* 4 360 (1951)

THE FRANKLIN INSTITUTE • Laboratories for Research and Development

F-2236

References (cont)

19. Societe d'Electro-chimie, d'Electrometallurgie, et des Acieries  
Electrique d'Ugine  
British Patent No. 590,392 7 April (1942)  
" " No. 594,681 6 July (1944)  
U. S. Patent No. 2,497,268 4 February (1950)
20. L. Weil, Tech. Moderne 44 65 (1952)
21. C. Kittel, Rev. Mod. Phys. 21 541 (1949)
22. A. Kussman and G. v. Rittberg, Metallkunde 41 470 (1950)
23. L. Weil, Fr. Patent 943,100, 27 September (1948)
24. L. Misch, Z Phys. Chem. (B) 22 49 (1935)
25. A. J. P. Meyer and P. Taglang, Compt. Rend. 232 1545 (1951)
26. R. J. Teitel and M. Cohen, J., Metals 1 Trans. 285 (1949)

THE FRANKLIN INSTITUTE • *Laboratories for Research and Development*

2236

DISTRIBUTION LIST

Number of  
copies

2	Research and Development Board Information Office Library Branch Pentagon Building Washington 25, D. C.
2	Chief of Naval Research Office of Naval Research Washington 25, D. C.  Attention: Physics Branch (Code 421)
11	Director Naval Research Laboratory Washington 25, D. C.  Attention: Technical Information Officer (Code 2000) (9 copies) Code 2021 (2 copies)
1	Commanding Officer Office of Naval Research Branch Office 346 Broadway New York 13, New York
1	Commanding Officer Office of Naval Research Branch Office American Fore Building 844 North Rush Street Chicago 11, Illinois
1	Commanding Officer Office of Naval Research Branch Office 1000 Geary Street San Francisco 9, California
1	Commanding Officer Office of Naval Research Branch Office 1031 East Green Street Pasadena 1, California

THE FRANKLIN INSTITUTE • *Laboratories for Research and Development*

2236

DISTRIBUTION LIST (continued)

Number of  
copies

2	Officer in Charge Office of Naval Research Navy No. 100 Fleet Post Office New York, New York
1	Chief, Bureau of Aeronautics Navy Department Washington 25, D. C. Attention: TD-4
1	Chief, Bureau of Ordnance Navy Department Washington 25, D. C. Attention: Technical Library, AD 3
1	Chief, Bureau of Ships Navy Department Washington 25, D. C. Attention: Code 324
2	Commanding General Engineer Research & Development Laboratories Fort Belvoir, Virginia Attention: Technical Intelligence Branch
2	Central Air Documents Office U. B. Building Dayton 2, Ohio
2	Director National Bureau of Standards Washington 25, D. C.

THE FRANKLIN INSTITUTE • *Laboratories for Research and Development*

2236

DISTRIBUTION LIST (continued)

Number of  
copies

1	Resident Representative Office of Naval Research c/o University of Pennsylvania 3320 Walnut Street Philadelphia 4, Penna.  Attention: Mr. S. Ferraris
1	Ordnance Research Laboratory State College, Penna.
1	Dr. R. C. Hermann 8621 Georgia Avenue Applied Physics Laboratory The Johns Hopkins University Silver Spring, Md.